Alexander Dallinger, Bsc.

Ultrathin, adhesive skin-contact electrodes

Master's Thesis
to achieve the university degree of
Master of Science
Master's degree programme: Technical Physics

submitted to

Graz University of Technology

Supervisor
Dr. Dott. Francesco Greco

Institute for Solid State Physics
Head: Univ.-Prof. Ph.D. Peter Hadley

Graz, December 2018

Affidavit

I declare that I have authored this thesis independently, that I have not used other than the declared sources/resources, and that I have explicitly indicated all material which has been quoted either literally or by content from the sources used. The text document uploaded to TUGRAZ-online is identical to the present master‘s thesis.

Date	Signature

Eidesstattliche Erklärung

Ich erkläre an Eides statt, dass ich die vorliegende Arbeit selbstständig verfasst, andere als die angegebenen Quellen/Hilfsmittel nicht benutzt, und die den benutzten Quellen wörtlich und inhaltlich entnommenen Stellen als solche kenntlich gemacht habe. Das in TUGRAZ-online hochgeladene Textdokument ist mit der vorliegenden Masterarbeit identisch.

Datum	Unterschrift

Acknowledgments

I would like to thank everybody who supported me during my thesis and I especially want to thank my supervisor Francesco Greco for his support and providing me with his knowledge on this topic.
I also like to thank *Umana Medical Technologies* for financing parts of thesis and providing materials and input for the experiments.
At the Institute for Solid State Physics I want to thank everybody who helped me and provided their expertise to me.
Special thanks go to my family and Janina Koß for the support and motivation they provided to my all the time.

Abstract

Skin is the biggest organ of the body and it can be used as an interface to record several bio-signals from within the body, as in the case of electrocardiography (ECG), electromyography (EMG) or electroencephalography (EEG), among others. To this purpose, so-called skin-contact electrodes (e.g. wet Ag/AgCl electrodes) are used in clinical practice for the recording. Such electrodes show several disadvantages especially as regards to their stability over long term and poor wearing comfort. The object of this thesis was to investigate a new class of ultrathin, soft, skin-contact electrodes from commercially available polymer substrates to pave the way for wearable personal health monitoring.

The electrodes are based on stretchable conductors which were produced by patterning conductive thin films on top of a soft and stretchable polymer substrate. For patterning the conductive film two methods were investigated, the first was ink-jet printing of conductive polymer inks and the second was laser induced carbon pyrolisis to create porous and/or fibrous carbon, which was transferred onto the stretchable substrate. The various fabrication parameters for these processes were studied and optimized, thickness and conductivity of these materials were characterized and their electromechanical properties were tested with a custom tensile test setup with integrated resistance measurement.

On top of a medical adhesive with a thickness of $33 \pm 2\,\mu m$ an ink-jet printed conductive film of conjugated polymer with a thickness of a few hundred nm was deposited for the so-called ink-jet printed conductors (IPC). These IPC have a conductivity ranging from 100 to 650 S/cm, depending on the used drop spacing for printing and the number of printed layers. IPC showed a poor stretchability of only a few percent strain. On the other hand, the laser induced carbon conductors (LICC) showed low conductivity ($< 100\,S/cm$) but a very high stretchability of over 30 % strain.
A combination of both conductors (IPC+LICC) showed a very promising combination of the benefits of both materials which resulted in a highly conductive and stretchable conductor.

A fully working ECG-electrode prototype for *Umana Medical Technologies* based on the IPC and embedding the necessary interconnections to a wearable monitoring system was furthermore prepared. The prototype was fully characterized and tested for recording of ECG signal on skin, in comparison with a standard Ag/AgCl electrode. The results showed very promising recordings with all the main features of an ECG signal observed and clearly identified.

Since the quality of biosignal recording is strongly affected by the constraints imposed by the connector and cables, especially in ultrathin devices, a novel approach for multilayered electrodes through Vertical Interconnect Accesses (VIAS) was investigated. To show that it is possible to make multilayer electrodes and therefore future fully integrated electrodes, a LED was embedded between two layers of medical adhesive and was contacted through the VIAS.

Contents

1. Introduction **1**
1.1. Objective . . . 2

2. Theory **3**
2.1. Epidermal Electronics . . . 3
2.2. Electrocardiography . . . 3
2.3. Mechanical Properties . . . 4
2.4. Conductive Polymers . . . 5
2.5. Laser Induced Carbonization . . . 5
2.6. Conductivity . . . 5

3. Experimental Setup **7**
3.1. Stretchable Conductors . . . 7
3.1.1. Medical Adhesive . . . 7
3.1.2. Inkjet printed Conductors . . . 8
3.1.3. Laser Induced Carbon Conductors . . . 11
3.2. Characterization of Thickness and Conductivity . . . 16
3.2.1. PEDOT:PSS . . . 16
3.2.2. LIC . . . 17
3.3. Electromechanical Stretching Setup . . . 18
3.3.1. Hardware . . . 19
3.3.2. Software . . . 21
3.3.3. Testing of Stretchable Conductors . . . 25
3.4. Electrocardiography . . . 28
3.4.1. Recording of ECG Signals . . . 28

4. Experimental Results **31**
4.1. Characterization of Conductive Inks . . . 31
4.1.1. Clevios^{TM} P JET700 . . . 31
4.1.2. Clevios^{TM} P JET700 N . . . 32
4.1.3. Comparison . . . 33
4.2. Laser Induced Carbonization . . . 34
4.2.1. Characterization of Laser Induced Carbon . . . 34
4.2.2. Morphology of Laser Induced Carbon . . . 35
4.3. Electromechanical Stretching Setup . . . 38
4.3.1. Calibration of the Load Cell . . . 38
4.3.2. Determination of Speed . . . 39
4.3.3. Verification . . . 40
4.4. Stretchable Conductors . . . 41
4.4.1. Medical Adhesive . . . 41
4.4.2. Ink-jet Printed Conductors . . . 43
4.4.3. Laser Induced Carbon Conductors . . . 45
4.4.4. Composite Conductor . . . 50
4.5. Electrocardiography Recording . . . 51

5. Miscellaneous **53**
5.1. Demonstrator for "Lange Nacht der Forschung" 53
5.2. Multi-layer Device through VIAS 53
5.3. Response to Humidity 56

6. Discussion and Conclusion **57**

Bibliography **59**

A. Room for Improvements **61**

B. Appendix **63**
B.1. Drop Spacing Conversion 63
B.2. Thickness Measurement of PEDOT:PSS Ink 63
B.3. How to Operate the Stretcher 64
B.4. ECG Recording Program 65

List of Figures

2.1. Description of peaks and intervals of an ECG recording, adapted from [4] . . 4
2.2. Chemical structure of PEDOT:PSS 5

3.1. Composition of the medical adhesive used as a substrate for the stretchable conductors 7
3.2. Stretchable conductor composed of a conductive layer and the medical adhesive (polyurethane + adhesive) as a substrate 8
3.3. Form of droplets depending on the liquid, clogging of nozzles and printing parameters, left = water droplets, right = PEDOT:PSS droplets 9
3.4. Wettability of the medical adhesive before (left) and after (right) hydrophilic surface treatment with plasma 10
3.5. Logo of the Institute of Solid State Physics drawn on top of polyimide with laser induced carbonization 12
3.6. Map of LIC depending on power and speed, Power = 50 % decreasing in 2 % steps, Speed = 10 % increasing in 10 % steps, 4 regions: destruction (high power, low speed), carbonization with fiber, carbonization, no carbonization (low power, high speed) [13] 13
3.7. Schematic representation of the four different areas produced by laser induced carbonization 14
3.8. Transfer of laser induced carbon onto medical adhesive to receive stretchable conductors 15
3.9. Comparison of not removed (left) and removed (right) carbon fibers and left over fibers marked with red arrows 15
3.10. Film of PEDOT:PSS with scratches for measuring the thickness of the film . 17
3.11. Sample of LIC with a removed part for measuring the thickness of the LIC film produced by laser induced carbonization 17
3.12. Conceptual drawing of the electromechanical stretching setup showing the main components of the system 19
3.13. Setup for calibrating the load cell with known weigths 20
3.14. Electromechanical test setup consisting of load cell (A), electrical contacts (B), sample (C) and movable stage (D) 21
3.15. Flowchart of the Stepper Controller software showing the basic functions and processes 23
3.16. Graphical User Interface: The connectivity panel in green (1), the manual control panel in red (2), the measurement control panel in blue (3), the graph area in violet (4) and the Log-Window in yellow (5) 24
3.17. Dimension of samples for electromechanical measurements with a conductor deposited onto the medical adhesive 26
3.18. Sample and paper frame mounted on the sample holders, the red rectangle marks the sample and the typical length 26
3.19. Four types of stretchable conductors which were tested for their electromechanical properties 27
3.20. Exemplary plot for the strain cycle of 30 % 28

3.21. Definition of interesting parameters for the stretchable conductors showing the starting resistance R_0, relative resistance ($\frac{R}{R_0}$)for the stretched and relaxed state 28
3.22. Placement of electrodes for ECG recording 29

4.1. Measurement results showing sheet resistance, thickness and conductivity over drop spacing and number of layers for the PJET700 ink 32
4.2. Measurement results showing sheet resistance, thickness and conductivity over drop spacing and number of layers for the PJET700N ink 33
4.3. A comparison of conductivity between the different conductive polymer inks printed with a drop spacing of 35 µm for 1, 3 and 5 layers 34
4.4. A comparison of the conductivity of all inks between the films on glass and on the medical adhesive (MA) printed with a drop spacing of 35 µm and 3 layers (thicknesses were assumed to be the same in both cases) 34
4.5. Measurement results showing sheet resistance, conductivity for LIC with a thickness of 8.7 ± 1.4 µm in carbon and transferred onto the medical adhesive 35
4.6. Morphology of the top surface of the carbon film produced with laser induced carbonization for LIC-Flat (left column) and LIC-Fiber (right column) . . . 36
4.7. Morphology of the bottom surface of the carbon film produced with laser induced carbonization which was transferred onto the medical adhesive to make it accessible 37
4.8. Morphology of the transferred LIC-Fiber produced with laser induced carbonization which was transferred onto the medical adhesive 38
4.9. Calibration curve for the load cell 39
4.10. Measurement curve for the determination of the speed in $\frac{mm}{s}$, linear up to a speed of 12 000 a.u. = 6.4 $\frac{\text{mm}}{\text{s}}$ 40
4.11. Comparison of tensile test of Elastosil® done by Wacker Chemie AG and Michael Gobald 40
4.12. Stress-strain plots for the four strain cycles showing plastic deformation and cyclic softening 42
4.13. Exemplary strain cycle over time and relative resistance change ($\frac{R}{R_0}$) over time and strain of one IPC 43
4.14. Pictures of one IPC showing its not stretched and stretched state taken with a microscope 44
4.15. Exemplary strain cycle and relative resistance change ($\frac{R}{R_0}$) over time of two very bad IPC 45
4.16. Exemplary strain cycle over time and relative resistance change ($\frac{R}{R_0}$) over time and strain of one LICC (LIC-Flat $\parallel$) 46
4.17. Pictures of one LICC (LIC-Flat $\parallel$) showing its not stretched and stretched state taken with a microscope 46
4.18. Exemplary strain cycle over time and relative resistance change ($\frac{R}{R_0}$) over time and strain of one LICC (LIC-Flat $\perp$) 47
4.19. Pictures of one LICC (LIC-Flat $\perp$) showing its not stretched and stretched state taken with a microscope 48
4.20. Exemplary strain cycle over time and relative resistance change ($\frac{R}{R_0}$) over time and strain of one LICC (LIC-Fiber) 49
4.21. Pictures of one LICC (LIC-Fiber) showing its not stretched and stretched state taken with a microscope 49

4.22. Exemplary strain cycle over time and relative resistance change ($\frac{R}{R_0}$) over time and strain of one composite conductor (LIC-Fiber + PEDOT:PSS) 50
4.23. Comparison between MA electrode prototype and a commercially available Ag/AgCl electrode 51
4.24. ECG recordings done with a commercially Ag/AgCl and a MA electrode . . 52

5.1. Pictures of the PEDOT:PSS VIAS taken with a SEM 54
5.2. PEDOT:PSS VIAS demonstrator with an LED embedded between two layers of medical adhesive 55
5.3. Sketch of an embedded ECG electrode realized with PEDOT:PSS VIAS for connecting the different layers 55
5.4. Array of LIC stripes on medical adhesive pasted onto a glass slide with copper contacts 56
5.5. Humidity response curve of the LICC 56

B.1. A measurement of thickness to show that the film surfaces of PJET700 and PJET700N are very rough and result in big uncertainties for the thickness . 63

List of Tables

3.1. Starting values of printing parameters for PEDOT:PSS 8
3.2. Laser engraver power and speed settings for the production of laser induced carbon without (LIC-Flat) and with fibers (LIC-Fibers) used for the LICC . 14
3.3. Parameters for the stretching cycles used to measure the electromechanical behavior of the stretchable conductors; Strain = initial length / displacement 27

4.1. Weights used for calibration and their measured values in grams 39
4.2. Conversion of common speed values form arbitrary units in $\frac{mm}{s}$ 40
4.3. Energy loss due to plastic deformation and heat dissipation according to equation (2.2) 42
4.4. Remaining plastic deformation after stretching and relaxing 42
4.5. Statistical results of the PJET700 conductor for different stretching cycles with R_0 the starting resistance and the relative resistance $\frac{R}{R_0}$ for the stretched and relaxed state 45
4.6. Statistical results of the PJET700N conductor for different stretching cycles with R_0 the starting resistance and the relative resistance $\frac{R}{R_0}$ for the stretched and relaxed state 45
4.7. Statistical results of the LIC-Flat $\parallel$ conductor for different stretching cycles with R_0 the starting resistance and the relative resistance $\frac{R}{R_0}$ for the stretched and relaxed state 47
4.8. Statistical results of the LIC-Flat $\perp$ conductor for different stretching cycles with R_0 the starting resistance and the relative resistance $\frac{R}{R_0}$ for the stretched and relaxed state 48
4.9. Statistical results of the LIC-Fiber conductor for different stretching cycles with R_0 the starting resistance and the relative resistance $\frac{R}{R_0}$ for the stretched and relaxed state 50
4.10. Statistical results of the composite conductor for different stretching cycles with R_0 the starting resistance and the relative resistance $\frac{R}{R_0}$ for the stretched and relaxed state 51

B.1. Conversion from drop spacing (DSP in µm) in DPI 63

Abbreviations

CA	Cellulose Acetate
DSP	Drop Spacing
ECG	Electrocardiography
EEG	Electroencephalography
EMG	Electromyography
IPC	Ink-jet Printed Conductors
LIC	Laser Induced Carbon
LICC	Laser Induced Carbon Conductors
MA	Medical Adhesive
PDMS	poly(dimethylsiloxane)
PEDOT	poly(3,4-ethylenedioxythiophene)
PI	polyimide
PSS	poly(styrenesulfonate)
VIAS	Vertical Interconnect Accesses

1. Introduction

The skin is the biggest and one of the most interesting organs of the body. Apart from being a barrier against pathogens and an interface across which chemicals and water can be exchanged, it can be thought as a big sensory organ sending signals of tactile and thermal stimuli to the brain, allowing us to sense our environment. Furthermore, by electrically interfacing with skin, it is also possible to obtain important information about our health condition. This information is for example about heart (electrocardiography ECG), muscle (electromyography EMG) or brain activity (electroencephalography EEG) and can be recorded with electrodes placed on the outer layer of skin: the epidermis. These skin-contact electrodes record electrical signals which permit the analysis of the functionality of different tissues and organs. Although the basic knowledge of electrophysiological mechanism and the technology of electrical devices for analyzing these signals made big progresses, the skin-contact electrodes used for electrically interfacing with skin remained basically unchanged for the last decades. For clinical uses, a wet electrode based on Ag/AgCl gel is used to establish the skin-electrode interface. Even though they are extensively used, they have a few disadvantages. The comfort while wearing is poor, due to the bulkiness and rigidity of the electrodes, the time stability and signal quality is not only limited by the drying of the gel but also by the factors which prevent a comfortable electrode. [1] [2]

On the contrary, future personal health monitoring devices should allow for a long term recording of bio-signals with integrated imperceptible devices on the skin. To make electrodes which ensure a comfortable, long term recording a few properties should be minded. The materials should be bio-compatible, imperceptible (thin and lightweight), stretchable, conductive and breathable for the skin.
Although the choice of materials is very critical, and the research is still going on to obtain materials which mimic the skin in mechanical properties, the focus of this thesis was to combine already available materials and processing techniques. A source for bio-compatible, breathable and imperceptible materials can be found in wound covers from medical application. These materials are not toxic and have been tested and used for a long time. Since they are made for enhancing the healing process of wounds the mechanical properties are very similar to the ones of skin and are predestined for an application of a substrate for these electronics.

Smartening (transforming into integrated electronics) these materials requires some technique which allows patterning of conductive thin films. The combination of the stretchable material and the conductive film results in a class of materials which is called stretchable conductors.
There are several processes which can be used to deposit thin layers of conductive materials. Two novel processes for patterning of conductive films were tested. One being ink-jet printing of conductive polymer inks and the other one was laser induced carbon which allows the drawing of conductive carbon tracks into a insulating polyimide sheet with the help of a commercially available laser engraver.
While the ink-jet printing needs some prior treatment of the hydrophobic surface to enhance printability, the laser induced carbon is embedded into the flexible but not stretchable polyimide and needs to be transferred onto the stretchable substrate.

The combination of the substrate and the conductive thin film can be used to create skin-contact electrodes which have mechanical properties similar to skin and enhance the contact of skin and electrode. One criterion for characterizing these skin-contact electrodes is their electromechanical behavior under certain levels of strain. Since skin is very soft and stretchable, the electrodes are exposed to a steady change of stretching and compressing. A way to measure the mechanical properties of materials is the tensile test where a sample is exposed to a certain strain and the stress is measured. The combination of this test with a simultaneous electrical resistance measurement gives insight into the electromechanical behavior of the studied material.

1.1. Objective

The objective of this thesis was to investigate materials and processes for fabrication of ultrathin, adhesive skin contact electrodes.

The thesis was split into four main parts:

1. Investigation of the substrate material, preferably a thin and flexible polymer and the investigation of the processes used to pattern conductive films onto the substrate
2. Designing and implementing an electromechanical testing setup to investigate the electromechanical properties of the produced stretchable conductors.
3. Development of a working prototype of an ECG-electrode for *Umana Medical Technologies* out of the ink-jet printed stretchable conductors
4. Preliminary investigation of Vertical Interconnect Accesses (VIAS) for multilayer electrodes

2. Theory

This chapter gives a basic review of the theories and methods used in this thesis. For a more sophisticated explanation please consult the references.

2.1. Epidermal Electronics

Epidermal electronics is a class of electronics which achieve a thickness, elastic modulus, bending stiffness and areal mass density matched to the epidermis. As a substrate thin elastic polymer sheets are used which can conformally adhere to the surface of the skin either through van der Waals interaction or through an applied adhesive depending on the thickness. A further property which the substrate should have is the one of gas-permeability, this allows the skin to breath while the device is applied. These epidermal electronics can be used to make devices incorporating light-emitting diodes, photodetectors, radio frequency inductors and other electronic components. For the power supply wireless coils or solar cells could be used.[3]

With this kind of electronics, it would be possible to make fully integrated sensor which can be placed onto the skin and measure signals regarding electrocardiography (ECG), electromyography (EMG) or electroencephalography (EEG) just to name a few.

For this three main problems have to be faced, firstly the choice of substrate material, secondly the conductive material and the deposition method and a last the connectivity to external devices. All three parts will be investigated in this thesis.

2.2. Electrocardiography

The process of recording the electrical activity of the heart is called Electrocardiography (ECG). Electrodes are placed on the skin which record small electrical changes (in the range of hundreds of µV) that arise from the heart muscle. These signals originate from the pattern of depolarizing and repolarizing of the muscle during each heartbeat.

Some parameters can be extracted from these recordings. The heart rate (HR) for example is the frequency of one complete heartbeat and is expressed as beats per minute (bpm). The Inter-Beat Interval is the distance between to individual beats of the heart (mostly the RR-interval, see figure 2.1).

In figure 2.1 a part of an ECG recording is shown. The different peaks and intervals are label which are used to interpret such a recording. For this thesis only a qualitative check of the ECG signal is done. This means that all the different peaks and intervals should be recognizable.[4]

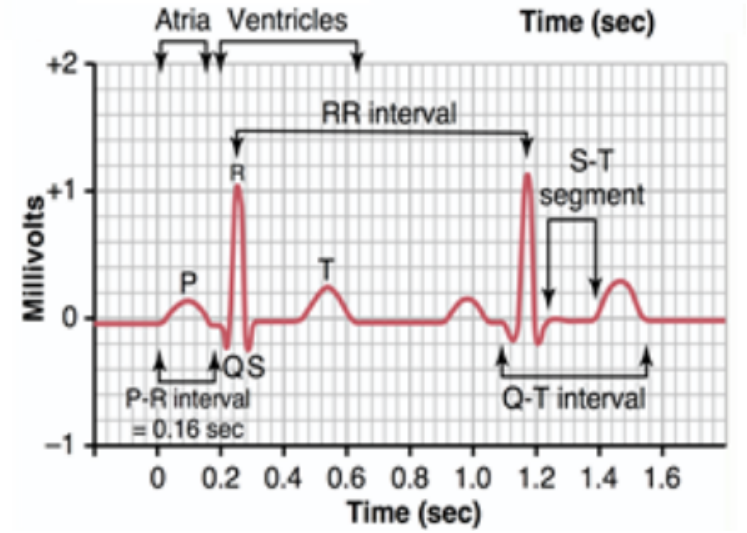

Figure 2.1.: Description of peaks and intervals of an ECG recording, adapted from [4]

2.3. Mechanical Properties

As stated before, the mechanical properties of skin and the substrate material for epidermal electronics should be, ideally, the same in order to maximize adhesion, durability and comfort.

Skin has a Young's modulus which ranges typically from 10 kPa to 0.1–0.5 MPa and is highly dependent on the relative humidity and temperature. Furthermore, it can sustain strains up to 140 % of strain before failure.[5]

One of the most used experiments for mechanical properties is the tensile test in which a sample is subjected to a controlled stress. Some information about the elastic or plastic behavior, Young's modulus and other mechanical parameters can be obtained. A typical setup is to fix one side of the sample to a load cell to measure the implied stress (σ) and elongate the sample to strain ($\epsilon = \frac{\Delta l}{l_0}$).

The Young's modulus (E) gives information about the stiffness of a material and is defined as:

$$E = \frac{\sigma(\epsilon)}{\epsilon} = \frac{F/A}{\epsilon} \tag{2.1}$$

Another parameter that can be extracted is the energy loss in the material. The area under the stress strain curve while stretching ($\uparrow$) is the energy put in the material and the area under the curve while unloading ($\downarrow$) is the released energy. In a purely elastic behavior these two would be the same and no energy is absorbed. But in the plastic behavior these two are different and energy is dissipated as heat.

$$Loss = \frac{\int(\uparrow) - \int(\downarrow)}{\int(\uparrow)} \tag{2.2}$$

2.4. Conductive Polymers

One of the most employed conjugated polymers is poly(3,4-ethylenedioxythiophene) doped with poly(styrenesulfonate) (PEDOT:PSS), an ionic and electronic conductor. It is available as a water based dispersion, which forms a continuous conductive film after the water is evaporated. This can be done through spin coating, drop casting or even ink-jet printing onto different substrates. PEDOT:PSS is used in antistatic coatings, as charge injection layers in OLED or could even be used in neural implants due to its recently proved biocompatibility.[6] Another advantage of PEDOT is its good electrical, chemical and thermal stability compared to some other conductive polymers. The reason why this polymers are conductive is that the electrons can easily jump within and between the chains of the polymer. This is indeed a rather simple explanation and in reality it is a combination of many factors. The conductivity reaches from a few S/cm to a few thousand S/cm.[7]
The stretchability of PEDOT:PSS films depends strongly on the formulation, used deposition methods and the pretreatment of the substrate surface. The group of Zhenan Bao reported a PEDOT:PSS film on poly(dimethylsiloxane) (PDMS) which was reversibly stretchable up to 30 % strain and even stayed reasonably conductive up to 188 % strain.[8][9]

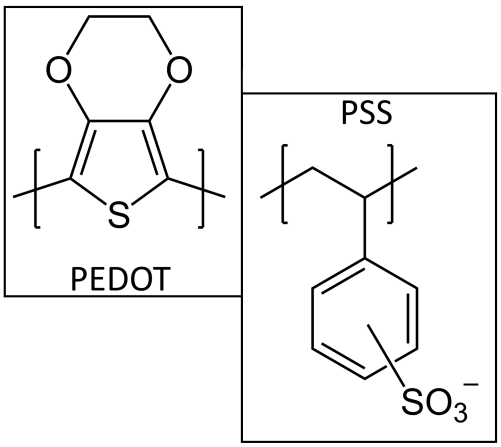

Figure 2.2.: Chemical structure of PEDOT:PSS

2.5. Laser Induced Carbonization

Graphene-based nanomaterials are used in many research fields and have been widely studied. Current synthesis strategies either need high temperatures or multi-stepped chemical synthesis routes. An alternative is the production of carbon through laser-induced pyrolisis of polyimide (PI) with a commercially infrared laser engraver. This is a one-step, fast, cheap and very scalable approach for the production of porous graphene or carbon. The sp^3-carbon atoms are converted to sp^2-carbon atoms through the photothermally activation with the laser. Carbon produced with this method shows a high electrical conductivity and can be used to easily scribe conductive patterns into the insulating PI. [10]

2.6. Conductivity

Conductivity is a very important parameter when talking about electronics. A common method for thin films is to measure conductivity indirectly in form of the sheet resistance

of a sample with a four-point probe and then calculate the resistivity with equation (2.3). For this the thickness t has to be known and should be measured. Equation (2.3) shows the relation of conductivity σ, resistivity ρ, sheet resistance R_S and the thickness t.

$$\sigma = \frac{1}{\rho} = \frac{1}{R_S t} \tag{2.3}$$

The sheet resistance is measured with a linear four-point probe and is obtained with equation (2.4). The first term ($\frac{\pi}{\ln(2)}$) is the geometry factor for an infinitely large, thin slice ($\frac{t}{s} << 1$, s ... probe spacing). This is true for the films in this thesis which have a thickness of less than 100 µm while the probe spacing is 1.25 mm. The second term is the measured resistance with the setup and the third term is a correction factor for the geometry of the sample.[11]

$$R_S = \frac{\pi}{\ln 2} \frac{\Delta V}{I} C_f \tag{2.4}$$

3. Experimental Setup

This section explains the methods and setups which were used in this thesis. The first part is about the methods with which the stretchable conductors were made. The second part is about the design and implementation of the electromechanical stretching setup which was used to measure the electromechanical properties of these stretchable conductors. The last part covers the topic of electrocardiography (ECG), how the ECG-electrode prototypes were manufactured and how the test measurements were performed.

3.1. Stretchable Conductors

In this thesis two different approaches on stretchable conductors were used. One method is to use an inkjet printer to deposit a conductive polymer ink on top of an insulating elastic polymer. The second method is to use a laser engraver to scribe conductive tracks of carbon into an insulating polymer, which is called a photothermal process [10]. Then this conductive tracks are transferred onto the elastic polymer. The elastic polymer was a medical adhesive (MA) which is discussed in the following section.

3.1.1. Medical Adhesive

As a substrate material for the stretchable conductors a commercially available transparent medical adhesive (Fixomull®) by BSN medical GmbH was used. The before defined properties for stretchable conductors are partly matched by this material. It is a stretchable polymer with an elastic behavior. Since it is used as a wound cover in medical applications it is also water impermeable but gas permeable to let the skin breath. The last property is the one of being imperceptible, with a thickness of $d = 33 \pm 2\,\mu m$ it easily follows the topography of the skin and is hardly felt by the wearer.
The medical adhesive is composed of 4 layers which are shown in figure 3.1. The first layer is a plastic liner on which the second, a polyurethane layer, was deposited during production. The second layer is covered with a polyacrylate adhesive layer for the adhesion to the skin. This layer is in turn covered by a paper liner for protection. To apply the medical adhesive to the skin, the paper liner is removed before it is placed on the skin and then the plastic liner can be removed.

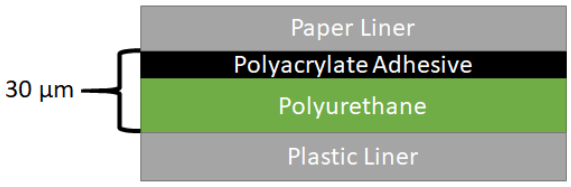

Figure 3.1.: Composition of the medical adhesive used as a substrate for the stretchable conductors

Based on the properties cited so far, this medical adhesive has been selected as a substrate for the fabrication of stretchable conductors. For a stretchable conductor, a conductive layer

had to be deposited on the material, this was done with the two methods mentioned before, resulting in IPC and LICC
So the produced stretchable conductors are composed of an insulating layer of elastic material (medical adhesive = polyurethane + adhesive) with a conductive layer on top as shown in figure 3.2.

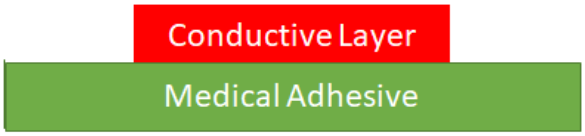

Figure 3.2.: Stretchable conductor composed of a conductive layer and the medical adhesive (polyurethane + adhesive) as a substrate

3.1.2. Inkjet printed Conductors

The inkjet printed conductors (IPC) were printed with a Dimatix Materials Printer DMP-2850 (FUJIFILM Dimatix, Inc.; USA) using a piezo inkjet cartridge with a drop volume of 10 pL.

Inkjet Printing

The ink was inserted into a printing cartridge with a syringe and a cellulose acetate (CA) membrane filter with a pore size of 0.2 µm in order to prevent clogging of the printing nozzles. The cartridge should be stored for a few hours to get rid of any air bubbles. After this the cartridge was mounted onto the printing head and placed in the printer.
Next, the printing parameters have to be set, this can be done with the printer software. Important parameters are the jetting waveform, jetting voltage, tickle frequency, meniscus vacuum, and the cleaning cycle.
The jetting waveform determines how the drops are created. This is done by controlling the electrical signal sent to the piezoelectric actuators and influences the formation of droplets. If set wrongly, no droplets are produced or the ink is sprayed around instead of being dropped. The jetting voltage determines the acceleration of the ink droplets, again if not set correctly the formation of droplets can be prevented. To prevent the ink from drying out the tickle frequency tickles the drops so that the fluid is always in motion. The meniscus vacuum acts against the gravity and helps to keep the droplets at the edge of the nozzles. When the nozzles are clogged it is possible to clean them with a cleaning cycle, this should not be used to often because a lot of ink is used during this process. A few values are given in table 3.1, but since the printing performance depends also on several environmental parameters such as temperature and humidity this values should only be used as a starting point for PEDOT:PSS inks.

Table 3.1.: Starting values of printing parameters for PEDOT:PSS

Printing Parameter	Value
Jetting Voltage	28 V
Tickle Frequency	5 kHz
Meniscus Vacuum	4 inches H_2O

The printer offers a drop watcher which makes it possible to observe the droplets as they are ejected from the nozzles. Figure 3.3 shows droplets of water (left) and droplets of PEDOT:PSS (right). The water droplets on the left are nearly spherical while the PEDOT:PSS droplets have a long tail trailing behind them. It is also clearly visible that the third water droplet is slower than the other two, this can be due to clogging of this nozzle. The different form comes from differences in viscosity and densities of the liquids.

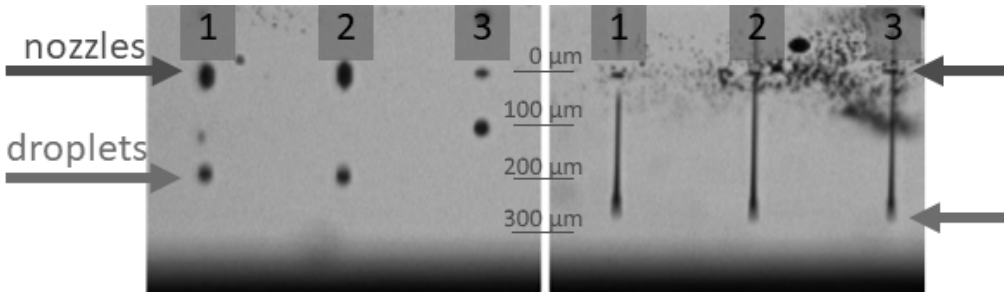

Figure 3.3.: Form of droplets depending on the liquid, clogging of nozzles and printing parameters, left = water droplets, right = PEDOT:PSS droplets

Once the parameters are set accordingly for droplets with constant speed and form, the printing pattern settings can be set. The printing pattern can either be set as a matrix of drops or can be imported from a black and white indexed bitmap.

The important parameter for the printing pattern is the drop spacing (DSP) in µm which represents the resolution of the printed pattern. It can be changed by adjusting the mounting angle of the printing head from 0° to 90° resulting in a drop spacing from 5 to 254 µm which means 5080 to 100 dpi (see table B.1 for some conversion values). A high drop spacing means that the individual ink droplets are deposited far apart one from each other on the substrate and it is not possible to get a complete coverage. If the drop spacing is set to small values, instead, the drops are deposited too close to each other, resulting in poor quality of the printed layer. Therefore, to get a good coverage and film quality the drop spacing should be finely tuned.

The quality of the film is not only dependent on the printing parameters but also on the substrate. If the substrate is rather hydrophobic the resulting film may not be very good since most inkjet printable inks are water based.

This problem arises with the medical adhesive when printing on the adhesive side. The polyacrylate adhesive is very hydrophobic and prevents good printing results. A strategy to decrease the hydrophobic properties was therefore needed and an air plasma treatment of the substrate prior to printing was investigated.

Indeed, an air plasma treatment it is possible to increase the surface energy, providing improved wettability. The substrate processed by a residual gas plasma and the surface undergoes oxidation due to the bombarding of plasma ions. This leads to formation of polar hydroxyl groups on the surface and enhances the substrates wettability, as displayed in figure 3.4. On the left side of the figure the untreated surface with aggregation of ink droplets can be seen. In contrast, the plasma treated surface on the right side shows a film of conductive ink which completely covers the surface.

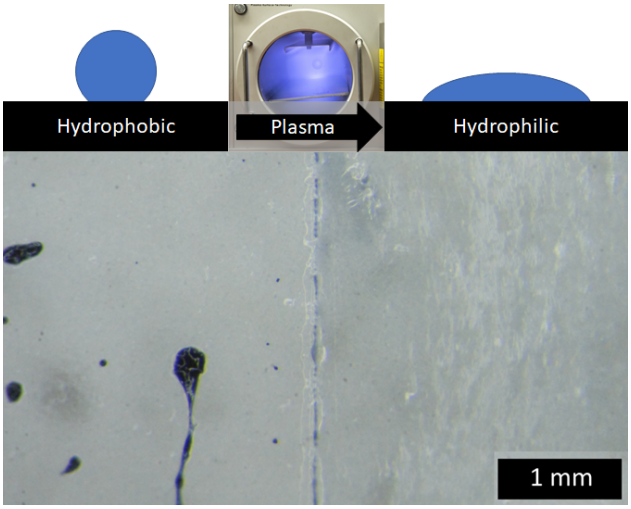

Figure 3.4.: Wettability of the medical adhesive before (left) and after (right) hydrophilic surface treatment with plasma

Inks and Parameters used for Inkjet Printed Conductors

For the inkjet printed stretchable conductors different formulations of water based PEDOT:PSS ink and printing parameters were used. The information for the Clevios® inks was taken from the Clevios-Heraeus homepage.[12]
The PEDOT:PSS inks which were used are the following:

- Clevios® PJET 700
  - Solid content: 0.6 to 1.2 %
  - Conductivity: > 650 S/cm
  - Viscosity: 5 to 20 mPa s
  - pH: 2 to 4
- Clevios® PJET 700 N
  - Solid content: 0.6 to 1.2 %
  - Conductivity: > 500 S/cm
  - Viscosity: 5 to 20 mPa s
  - pH: 5 to 8

The two inks are from Heraeus and are called Clevios® PJET 700 and the neutral formulation PJET 700 N.
A commonly encountered problem in printing with the normal PJET700 ink is that it is rather acid and tends to destroy the printing heads. Therefore the neutral formulation PJET700N, which should not have this problem, was also included in the characterization.
As described before all inks were filtered with a CA membrane filter (pore size = 0.2 µm) before the printing. The cartridge was then left for a few hours to degas ink from air bubbles.
Regarding the printing parameters the drop spacing (DSP) and the number of layers were varied. For the drop spacing and number of printed PEDOT:PSS layers three values were chosen:

- DSP = 25, 35 and 45 µm

- Layers = 1, 3 and 5

For these values the characterization regarding thickness and conductivity were made. The experimental setup for this measurements can be found in *Section 3.2 Characterization of Thickness and Conductivity* and the results are shown in *Section 4.1 Characterization of Conductive Inks*.

The results from the conductivity characterization were used to set printing values for the stretchable conductors which were tested later on (see *Section 3.3.3 Testing of Stretchable Conductors* and for results *Section 4.4 Stretchable Conductors*).

3.1.3. Laser Induced Carbon Conductors

The laser induced carbon conductors (LICC) were produced with the commercially available laser engraver VLS 2.30 from Universal Laser System. It is a 30 W CO_2 laser with a wavelength of 10.6 µm and a maximum speed of 1.6 $\frac{m}{s}$. The lens used in this study was the HPDFO lens with a focused spot size of 30 µm.

In the following paragraphs the process of creating laser induced carbon (LIC) on top of polyimide (Kapton®) and the method of transfer onto the medical adhesive are explained.

Laser Induced Carbonization

Laser Induced Carbonization is a photothermal process and depends on the used laser fluence ($\frac{J}{m^2}$). The heat generated by the laser irradiation thermally converts the sp^3-carbon atoms to sp^2-carbon atoms and results in laser induced graphene.[10]

The fluence can be seen as a combination of used power and speed for the laser engraver. All values are given in percent and can be calculated back with the values given before. So a high power and a low speed means a high fluence and a high deposition of energy in our substrate. Certain settings can result in the same fluence despite having different power and speed settings. As a substrate a commercially available polyimide sheet (Kapton®) with a thickness of 50 µm was used. The main advantage of this method is the possibility to contactless draw conductive patterns on top of an insulating material. The figure 3.5 shows the Institute of Solid State Physics logo as carbonized area on top of the polyimide film.

Figure 3.5.: Logo of the Institute of Solid State Physics drawn on top of polyimide with laser induced carbonization

Power Settings for Laser Induced Conductors

To find the right settings for formation of laser induced carbon on polyimide a trial and error approach was used. Some starting values for this investigation were taken from [10].

A more methodological approach for this topic was done by Jürgen Mitterling in his bachelor thesis [13]. Figure 3.6 shows a map of laser induced carbon depending on power and speed settings done in that study. The top row starts with a setting of power = 50 % and speed = 10 %. The speed is increased in 10 % steps up to 100 % and the power is decreased in 2 % steps down to 20 %. At a first glance three regions can be distinguished, the region on the lower right corner where no carbonization took place (blue border), a region in the middle section were carbonization took place and a region on the left side were the polyimide got destroyed (red border).

When taking a closer look at the region where carbonization takes place it is possible to distinguish sub regions. At the border to the region where no carbonization takes place (blue border) a flat carbon surface is produced. Going to higher fluences fibers begin to emerge from the surface and at the border to the region where destruction occurs (red border) these fibers become very long with length up to 1 mm. The border between the region of flat carbon (also carbon with microscopic fibers) and macroscopic fibers is loosely marked by the green border. A schematic representation of the four regions (no carbonization, carbonization, fiber, destruction) is shown in figure 3.7.

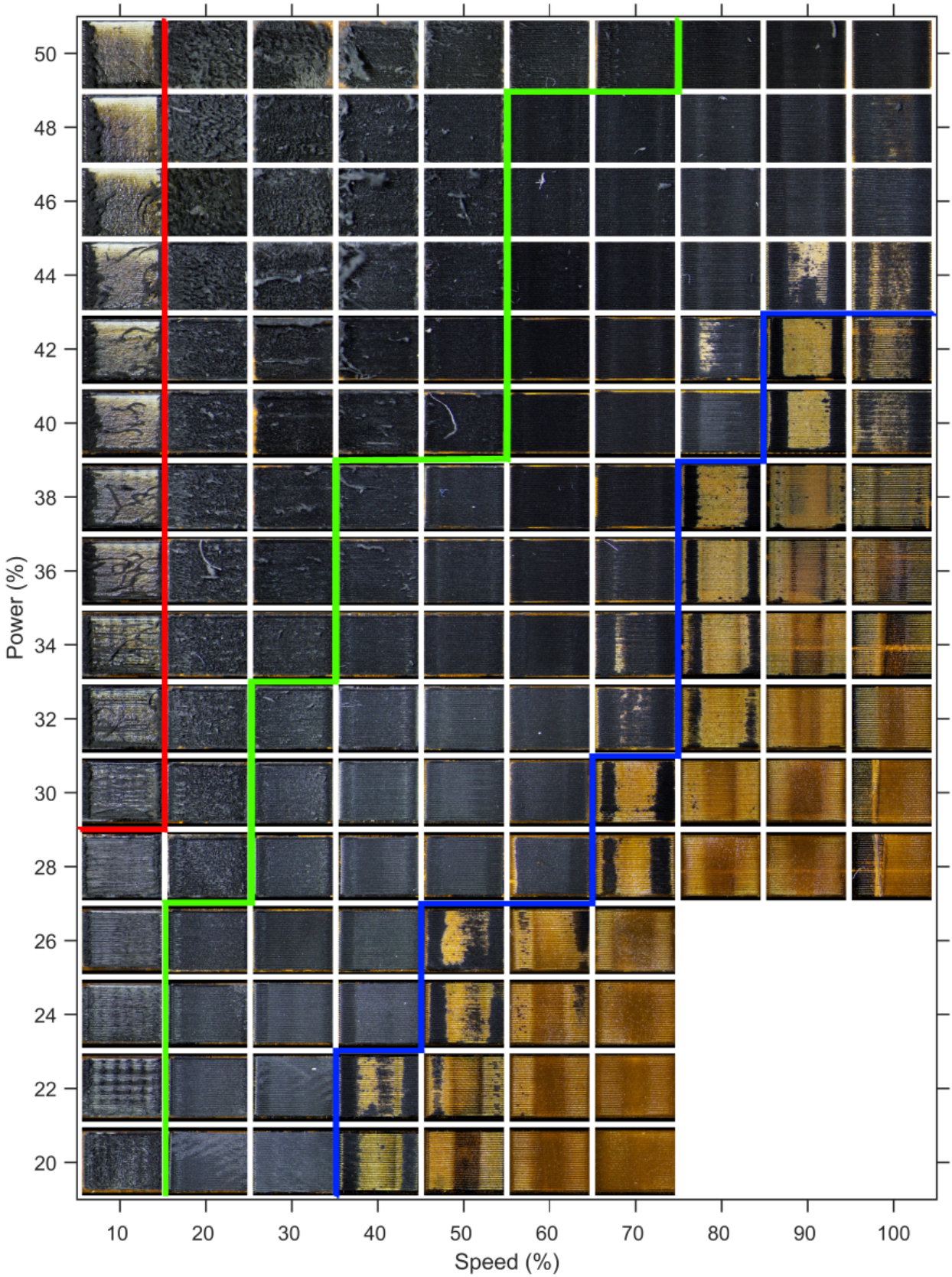

Figure 3.6.: Map of LIC depending on power and speed, Power = 50 % decreasing in 2 % steps, Speed = 10 % increasing in 10 % steps, 4 regions: destruction (high power, low speed), carbonization with fiber, carbonization, no carbonization (low power, high speed) [13]

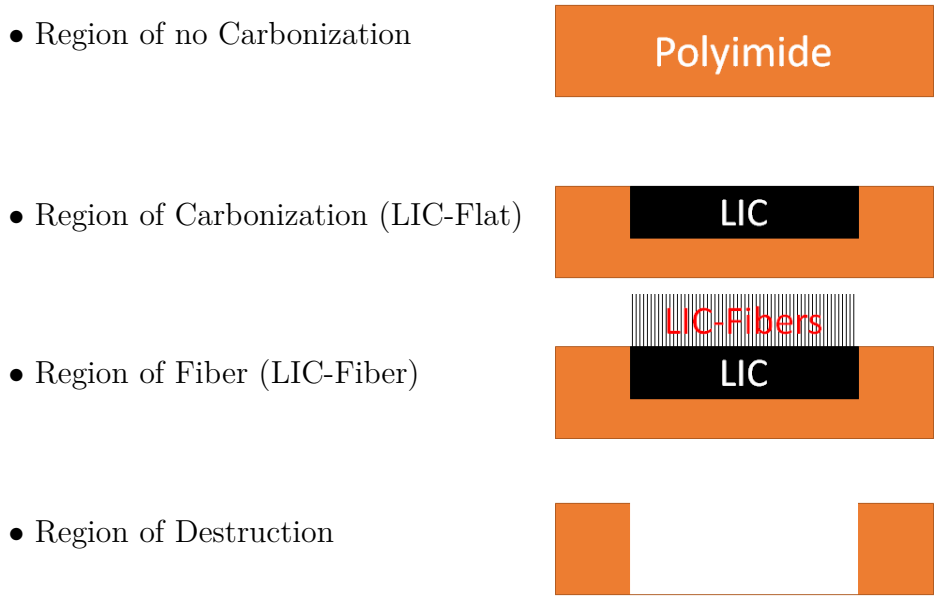

Figure 3.7.: Schematic representation of the four different areas produced by laser induced carbonization

For the stretchable conductors made from laser induced carbon two settings were used (see table 3.2). One setting for a formation of carbon without fibers (LIC-Flat) and a setting for a formation of carbon with fibers (LIC-Fiber).
The polyimide was fixed onto a metal plate with a thickness of 1 mm by stripes of double-sided adhesive tape. The focus was accidentally set to 2 mm instead of 1 mm for the thickness of the plate. However, this turned out to be a good setting to obtain carbon fibers since the setting with a focus of 1 mm barely gave fibers at all. A similar behavior was observed in a recent paper [14]. The resolution was set to 500 PPI and an Image Density of 5. The Image Density determines the density of the raster lines used by the laser engraver while lasering.

Table 3.2.: Laser engraver power and speed settings for the production of laser induced carbon without (LIC-Flat) and with fibers (LIC-Fibers) used for the LICC

	Power	Speed
LIC-Flat	10 %	10 %
LIC-Fiber	20 %	10 %

For the LIC-Flat two different manufacturing methods were tested. Since the laser engraver has a preferential direction for lasering (making lines from left to right and back), samples with lines along the stretching direction (LIC-Flat $\parallel$) and samples with lines perpendicular (LIC-Flat $\perp$) were made.
For the two settings used for the production of the LICC, SEM imaging of the carbon surface was performed with an JEOL JSM-6490LV Scanning Electrode Microscope (SEM) operating at an acceleration voltage of 5 to 20 kV. The images and exact settings can be found in *Section 4.2.2 Morphology of Laser Induced Carbon.*
Also a characterization regarding the thickness and conductivity of the carbon layer was attempted, the methods can be found in *Section 3.2 Characterization of Thickness and*

Conductivity and the results in *Section 4.2.1 Characterization of Laser Induced Carbon*

Transfer of Laser Induced Carbon

To get a stretchable conductor the LIC has to be transferred from the rigid polyimide to the stretchable medical adhesive. For the LIC-Flat the whole carbon is transferred onto the medical adhesive (see figure 3.8a) and for the LIC-Fiber only the carbon fibers are transferred onto the medical adhesive (see figure 3.8b). To ensure that only the fibers are transferred only a certain pressure must be applied while transfer. After transfer of the fibers only the bulk carbon should be left over, the difference can be seen in figure 3.9. On the left is the intact carbon with fibers (darker region) and on the right there is the leftover bulk after removal of the fibers (lighter region). Another thing to notice is that not all fibers get transferred and are still visible on the right side (marked with the red arrows).

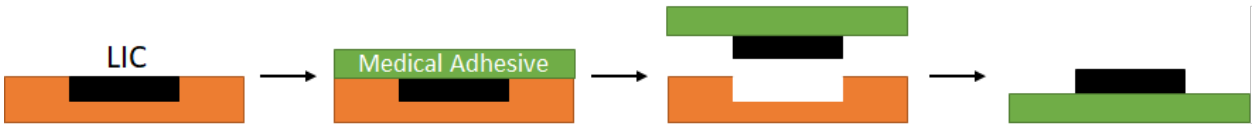

(a) Transfer of LIC-Flat onto medical adhesive

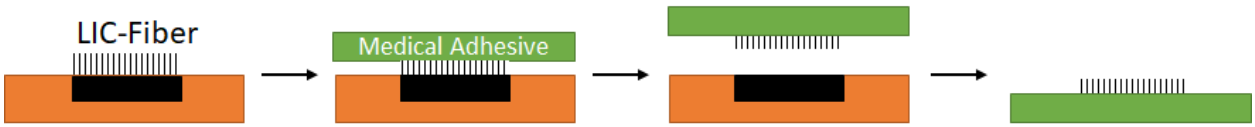

(b) Transfer of LIC-Fiber onto medical adhesive

Figure 3.8.: Transfer of laser induced carbon onto medical adhesive to receive stretchable conductors

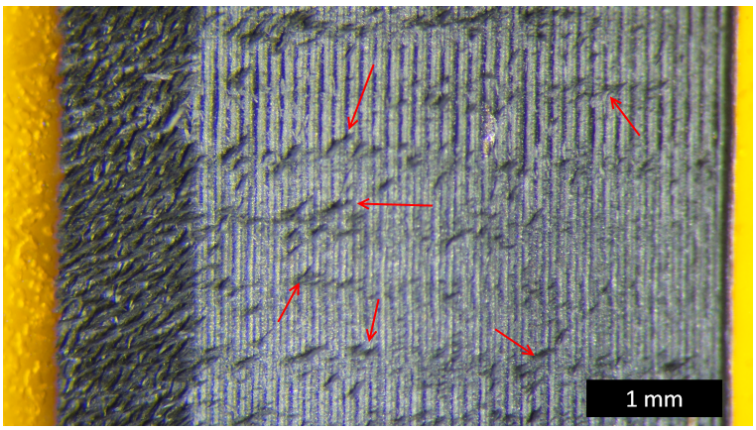

Figure 3.9.: Comparison of not removed (left) and removed (right) carbon fibers and left over fibers marked with red arrows

The exact sample dimensions and preparation for the LICC samples used for the electromechanical measurements can be found in *Section 3.3.3 Testing of Stretchable Conductors*.

3.2. Characterization of Thickness and Conductivity

The measurement of thickness was done with a stylus profilometer AlphaStep D-500 from KLA-Tencor. The length of the measurement for the thickness was around 1 to 2 mm depending on the sample. The speed for the measurement was set to 0.1 $\frac{\text{mm}}{\text{s}}$ and the force set to 1 mg. For the three samples at least five measurements per sample were done.

The conductivity was calculated according to equation (2.3) with the measured thickness and the sheet resistance which was measured with a custom four-point probe setup. The four-point probe setup uses a Keithley 2602B and four linearly arranged measurement tips with a distance of $d_{\text{probes}} = 1.5\,\text{mm}$. A current of around 1 mA was used to measure resistance of the sample. The current was slightly varied depending on the resistance of the sample. The samples used for measurements were squares with a length of 10 mm of ink or conductive carbon on either the glass substrate or the medical adhesive.

Equation (2.4) was used to determine the real sheet resistance with the help of correction factors depending on the sample thickness and geometry. [11]

3.2.1. PEDOT:PSS

For the PEDOT:PSS inks the thickness could only be measured for films printed on glass substrates because the adhesive side of the medical adhesive was too soft to be measured by the stylus profilometer and no other method was available.

For the measurement a PEDOT:PSS film was deposited onto the glass substrate with the inkjet printer and was dried (100 °C for 1 h). Then the sheet resistance measurement was performed and the same samples were prepared for the thickness measurement. For this, lines of ink were scratched away from the substrate with a needle. These lines were used as a reference point for the thickness of the film (see figure 3.10). The measurement was done across the two lines as shown in the figure.

The sheet resistance measurement was done for all parameters on samples deposited on the glass substrate and for selected parameters on samples deposited on the medical adhesive. For the calculation of the conductivity the thicknesses for both films were assumed to be the same.

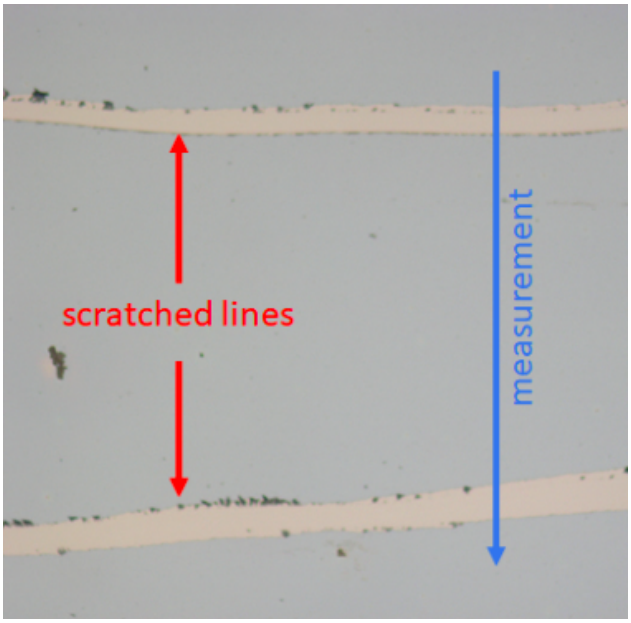

Figure 3.10.: Film of PEDOT:PSS with scratches for measuring the thickness of the film

The values for thickness and conductivity can be found in *Section 4.1 Characterization of Conductive Inks*.

3.2.2. LIC

The conductivity of the laser induced carbon was measured, like the one for PEDOT:PSS, with the four point probe. After this the thickness was measured after removing all the carbon with an adhesive tape and using the stylus profilometer to measure the remaining valley as shown in figure 3.11. On the left side the LIC still on the sample is displayed, while on the right side the sample after LIC removal is displayed. The arrows indicate that the measurements were done from the edge to the center of the sample. The reference was the surface of the polyimide.

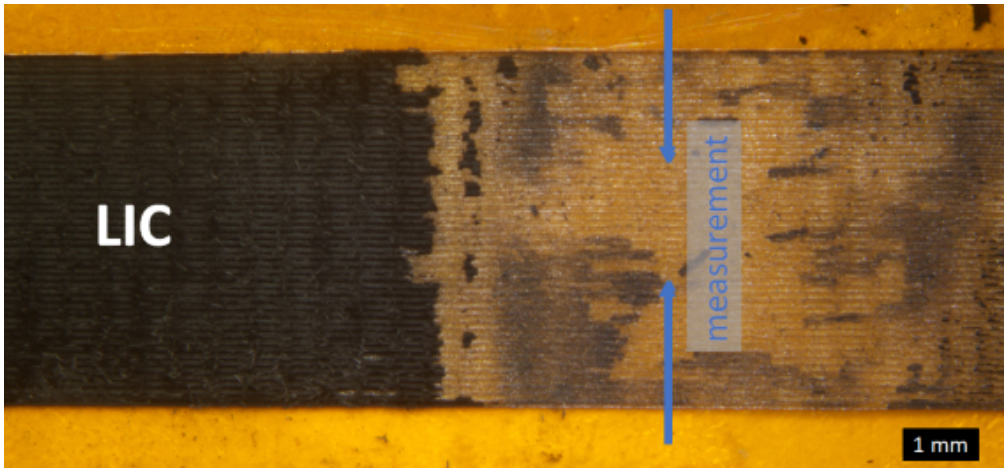

Figure 3.11.: Sample of LIC with a removed part for measuring the thickness of the LIC film produced by laser induced carbonization

The values for thickness and conductivity can be found in *Section 4.2.1 Characterization of Laser Induced Carbon*.

3.3. Electromechanical Stretching Setup

One of the main tasks of this thesis was to design and implement a setup to test stretchable conductors and other materials regarding electrical and mechanical properties.

The requirements for the setup are discussed in the following. The first requirement was the possibility to impose and measure a stress on the sample. The second requirement was the possibility to make electrical measurements while imposing a stress. As a last requirement an easy to use graphical user interface (GUI) and a simple measurement cycle editor were set.

This section is about the hardware and software used to design this setup.

The conceptual drawing in figure 3.12 shows the main components of the system. The sample gets mounted between two holders, one holder is fixed to a stage which is movable by a stepper motor. The other sample holder is fixed to a load cell to measure the stress imposed on the mounted sample. The signal from the load cell gets amplified, read out and converted to a digital signal at an analog input at the Arduino microcontroller. The stepper motor is driven by a stepper driver, which is connected via digital pins to the Arduino. The measured signals get transferred via USB to a PC where a programmed software (see *Section 3.3.2 Software*) processes the data. The graphical user interface (GUI) of the software enables the user to input a measurement cycle consisting of the following parameters:

- Strain in %
- Speed in arbitrary units
- Delay in ms

This cycle can be repeated or combined with other cycles of a different strain, speed or delay. Once saved into a so-called "Stretch File" it can be reused and modified. This file is translated and send as commands via USB to the Arduino where it is processed (explained in *Section 3.3.2 Software*).

At a specific time interval, the Arduino measures the force imposed on the sample and the position of the stage. When this data is sent to the GUI, the Keithley source meter gets triggered and measures the electrical resistance between the sample holders.

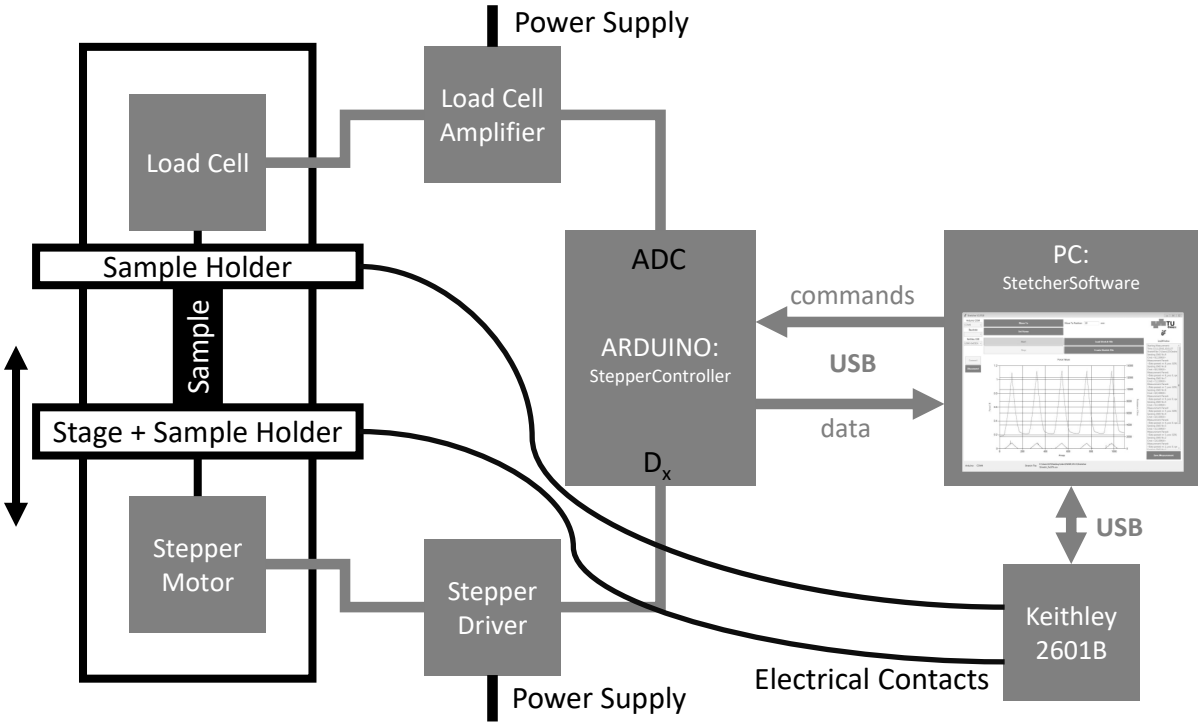

Figure 3.12.: Conceptual drawing of the electromechanical stretching setup showing the main components of the system

3.3.1. Hardware

The hardware used for the setup comprised the following:

- Load Cell Futek LRF400 + Amplifier Futek IAA100
- Linear Stage drylin® SHTC-12 + NEMA 17 Stepper Motor
- Keithley 2601B Source Meter
- Stepper Driver Allegro A4988 on Big Easy Driver board
- Arduino Uno Microcontroller

Load Cell

As explained before, the load cell measures the force acting on the sample. For the measurements, a load cell with a maximum load of 1.1 N was used in tension mode (Model Nr.: FSH00259). If a higher load should be measured, it is possible to replace the load cell with a different version with a higher capacity. Before the first use, the load cell amplifier needs to be calibrated for the load cell and should be checked from time to time. The calibration steps are from the Quick Start Guide for the IAA100 amplifier and are the following:

1. Set the excitation voltage DIP switch
2. Set the Gain DIP switch according to the sensors mv/V
3. With the sensor and amplifier completely connected apply the source voltage

4. With no load on the sensor adjust the Zero potentiometer until the output is close to 0 V

5. With a known load applied on the sensor adjust the Span potentiometer to the appropriate output level

6. Remove the load and reconfirm the zero load output, reapply known load and reconfirm the span output

The known weight is connected to the load cell via a pulley as shown in figure 3.13.

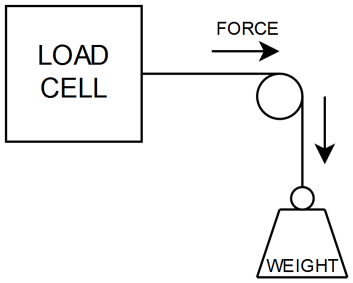

Figure 3.13.: Setup for calibrating the load cell with known weigths

Linear Stage

The linear stage, a premade kit from IGUS® was upgraded with a NEMA 17 stepper motor. This motor is driven by a stepper driver (Big Easy Driver) from Sparkfun and is connected to the Arduino via a self-made connector board.

The finished setup shown in figure 3.14 consists of the load cell (A), sample holder with the electrical contacts (B), sample (C) and movable stage (D). The electrical contacts are connected to the Keithley source meter for the resistance measurement.

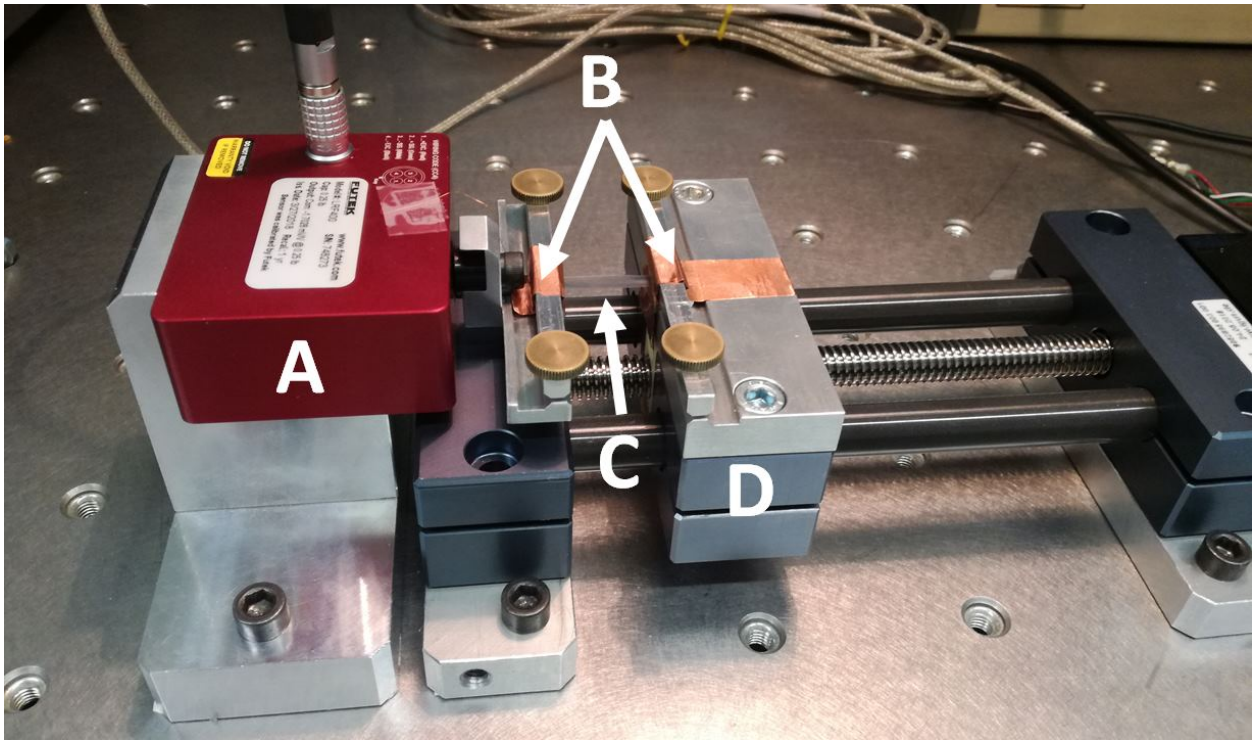

Figure 3.14.: Electromechanical test setup consisting of load cell (A), electrical contacts (B), sample (C) and movable stage (D)

3.3.2. Software

The software consists of two parts, one part is the "Stepper Controller" which is the Arduino program and interprets the commands sent from the computer. The second part is the "Stepper Software", the interface for the user. With this program, it is possible to define measurement cycles (so-called "Stretch-Files"), manually move the stage or save the measured data. The two programs communicate via Serial communication with a baud rate of 115 200 Bd.

Stepper Controller

The Stepper Controller is an Arduino sketch which is used to interpret commands sent from the user interface running on a computer. A command or transmitted data always starts with a "<" maker and ends with a ">" maker. This makes sure that no data is misinterpreted when something is lost. The command for the Arduino consists of four parameters separated by a comma: command number (CMD), position (POS), speed (SPD) and delay (DL).
A valid command looks like this:

<CMD,POS,SPD,DL>

When a new command arrives at the Arduino, a flag gets set and the command gets parsed. The CMD is saved in cmdValues[0], POS in cmdValues[1] and so on. The code snippet for the corresponding part is shown in listing 3.1.

```
void parseData(){
char * token;
//seperation of the parts into tokens and converting them to float
token = strtok(receivedChars,",\0");
for(int i = 0; i<4; i++){
cmdValues[i] = atof(token);
token = strtok(NULL,",\0");
}
//convertion of pos /mm to steps
cmdValues[1] = cmdValues[1]/2 * 200 *16;
char text[60];

//Feedback for LOG-Window
snprintf(text, 60,"<Data parsed: nr: %ld, pos: %ld, speed: %ld, wait: %
    ld>",(long)cmdValues[0],(long)cmdValues[1],(long)cmdValues[2],(long)
    cmdValues[3]);
Serial.println(text);

newData = false; //reset the newData flag
}
```

Listing 3.1: Code snippet of the parsing code which interprets the incoming commands from the user interface

Once the parsing is finished the command has to be interpreted. The command number (CMD) determines the action, numbers greater than zero are normal commands which result in a movement of the stage corresponding to POS, SPD and DL. Command numbers smaller than zero are special commands such as setting the home position or are reserved for future features. Listing 3.2 shows the main functions used to control the stepper motor and move the stage one step.

```
stepper.moveTo((long)cmdValues[1]);       // set end position = POS
stepper.setSpeed(cmdValues[2]);   // = SPD
if(stepper.distanceToGo()){       // step until position is reached
        stepper.runSpeedToPosition(); //step
}
```

Listing 3.2: Code snippet for moving the stage one step in the direction to POS, using SPD

After the step, if the measurement timer triggers a measurement, the Arduino reads out the current force and position and sends them to the Stepper Software where they get processed and displayed. After the stage reaches its position and the delay (DL) is greater than zero, the Arduino waits for this time and then sends a “Next-Command” back to the Stepper Software to request the next command. If it was the last command (CMD = 0) the Arduino sends back a “Finished-Command” to signal that it has finished all operations.

The basic functions and processes explained before are visualized as a flowchart in figure 3.15.

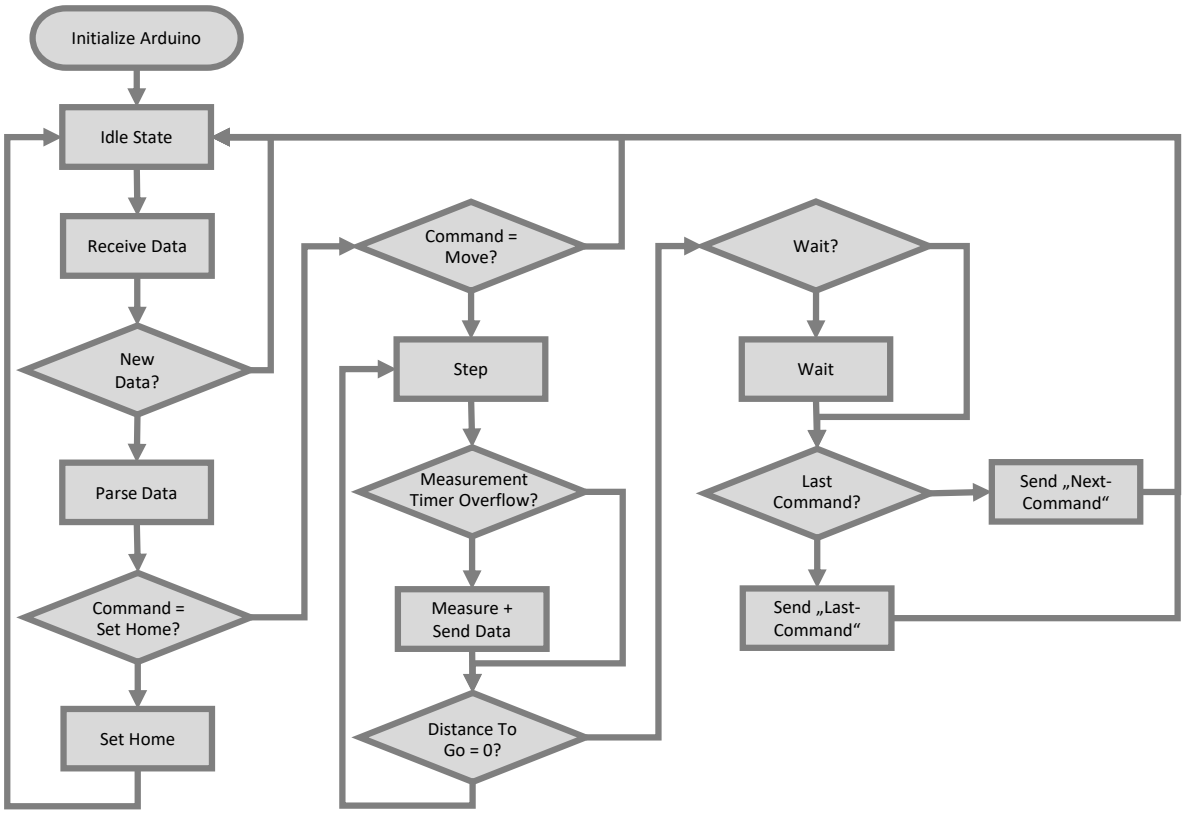

Figure 3.15.: Flowchart of the Stepper Controller software showing the basic functions and processes

Stretcher Software

The software for the user is called Stretcher Software which is a C# graphical user interface (GUI). It is connected to the Arduino via USB Serial communication and via USB to the Keithley source meter for the resistance measurement. C# was chosen because the Keithley needs a lot of driver software which can be easily packed into the installation file and is very easy to handle.

The GUI, shown in figure 3.16 has five different regions. Number 1 in green shows the connectivity panel where the ports and addresses of the Arduino and Keithley are set. The red area (2) is the manual control panel, where the stage can be manually moved to a position or the home position can be set. The third area in blue is the measurement control panel, where a Stretcher-File can be created or loaded and the measurement can be started or stopped. The violet area (5) displays the ongoing measurement, the force in newton in blue and the resistance in ohm in red. The last panel in yellow (5) is the Log-Window where all commands are logged. The “Save Measurement” button saves the measured data and the log into a .csv file (a more detailed explanation later).

Figure 3.16.: Graphical User Interface: The connectivity panel in green (1), the manual control panel in red (2), the measurement control panel in blue (3), the graph area in violet (4) and the Log-Window in yellow (5)

After creating and loading a Stretch-File the measurement can be started. The program prompts the user to input the dimension of your sample to include them in the results file. Now a command consisting of the four parameters <CMD,POS,SPD,DL> is sent to the Arduino and is executed. When the Arduino sends back measured data like force and current position, a flag is set and the GUI communicates with the Keithley to measure the resistance of the sample. Now all data is processed and displayed at the graph area. Once the Arduino has finished its task it sends either a “Next” or “Finished” command back. Now the GUI response with a new command or prompts the user to save the measured data in case the last command was sent.

Stretch-File

As explained before, a Stretch-File consists of multiple commands saved in .csv file. The first value is the strain in % to go to (POS), the second value is the speed (SPD), and the last value is a delay when the position is reached (DL). The command number (CMD) is added by the program since it depends on the number of commands (starting at N-1, where N is the number of commands and ending at 0 for the last command).
Listing 3.3 shows an example for a Stretch-File for one cycle to 100 % strain with a speed of 1000. The speed is an arbitrary unit since the real speed depends on various factors, it was measured after the setup was finished and can be found in *Section 4.3.2 Determination of*

Speed.

```
100,1000,1000
0,1000,1000
```

Listing 3.3: Example of a Stretch-File for a cycle to 100 % strain and back with a speed of 1000 (arbitrary units) and a delay of 1000 ms after each position

Result File

After the last command was sent and processed by the Arduino it sends back the "Finished" command and the user is prompted to save the measurement. The resulting file contains the measured data and at the end, a log is appended (see listing 3.4). The first row is the date and time plus the Stretch-File with which the measurement was executed. The measurement data consists four columns containing the time in milliseconds, position in millimeter, force in newton and the resistance in ohm (starting with line 2). Then there is the log section (line 8) which starts with "LOG_FILE:", at first there is the sample dimension with the length l0, the width b0, and the thickness d0. Then the starting resistance R0, followed by the log data from the log window (line 13) of the GUI are listed. This contains the commands sent to the Arduino and its response.

```
1  14.11.2018_10:18:29C:\Users\...\Stretch_5x5%.csv
2  Time / ms, Position / mm , Force / N , Resistance / Ohm
3  37094411.8001,0.0175,0.00313388671875,1010.52
4  37094440.8001,0.035625,0.00313388671875,1019.04
5  ...
6
7  LOG_FILE:
8  l0 / mm,18.9
9  b0 / mm,5
10 d0 / mm,0.03
11 R0 / Ohm,1005.3618
12 Starting Measurement
13 Time: 14.11.2018_10:18:12
14 StretchFile: C:\Users\...\Stretch_5x5%.csv
15 Sending CMD Nr.:9
16 Cmd: <9,0.945,1000,0>
17 Measurement Parsed:
18 <Data parsed: nr: 9, pos: 1512, speed: 1000, wait: 0>
19 Sending CMD Nr.:8
20 Cmd: <8,0,1000,0>
21 ...
```

Listing 3.4: An Example of a result file containing the measurement data and a log section (line 8) at the end

3.3.3. Testing of Stretchable Conductors

For the electromechanical measurements with the stretcher, samples with a dimension of 40 mm × 5 mm were prepared. On these samples the conductors were either printed (PE-

DOT:PSS) or transferred (LIC), the dimension of the conductor was 30 mm × 5 mm as shown in figure 3.17.

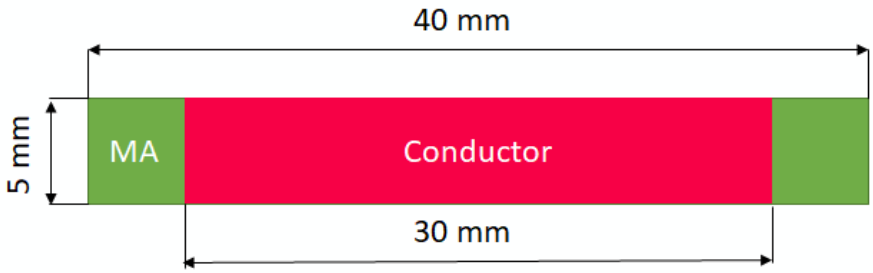

Figure 3.17.: Dimension of samples for electromechanical measurements with a conductor deposited onto the medical adhesive

These samples were placed on a paper frame for better handling while placing in the sample holders. The typical length after fixing the samples in between the holders was around 20 mm.
In figure 3.18 the sample and the paper frame are mounted on the sample holders. The red rectangle marks the sample and the typical length.

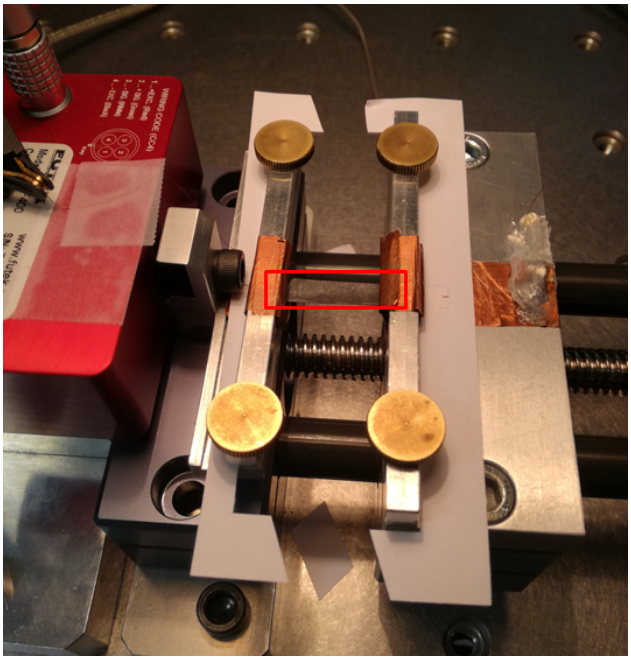

Figure 3.18.: Sample and paper frame mounted on the sample holders, the red rectangle marks the sample and the typical length

The electromechanical measurements were done for both stretchable conductors (IPC and LICC). For the IPC the PEDOT:PSS inks PJET700 and PJET700N and for the LICC the two LIC-Flat and the LIC-Fiber samples were measured. Also, a combination of PEDOT:PSS and LIC-Fiber (for results see *Section 4.4.4 Composite Conductor*) was made and measured. A symbolic overview of all samples is shown in figure 3.19.

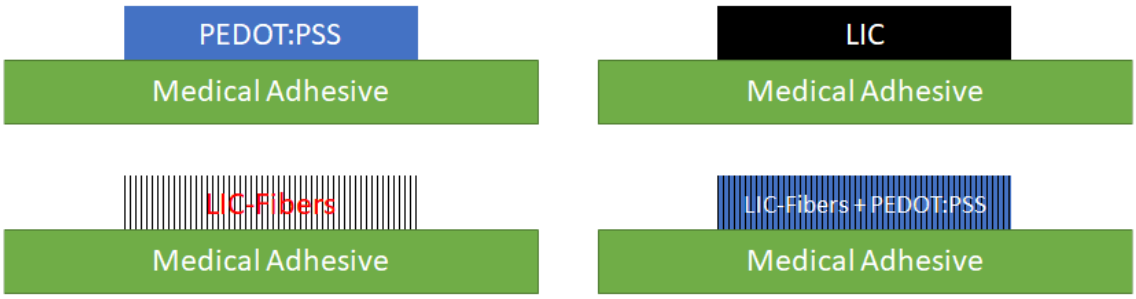

Figure 3.19.: Four types of stretchable conductors which were tested for their electromechanical properties

The stretching cycles set with the stretcher software are given in table 3.3. All cycles were tried to be used until the samples were broken and no resistance could be measured anymore. Particularly the cycle with 100 % strain was only used for samples which were working up to 30 % and it was included in the characterization to see the behavior at extreme strains.

Each strain cycle was applied to the sample one after the other so the effects of one cycle will be present in the following one. This was done because of time and practical reasons, also for the electromechanical behavior this should not be a problem.

Table 3.3.: Parameters for the stretching cycles used to measure the electromechanical behavior of the stretchable conductors; Strain = initial length / displacement

Strain (%)	Speed (a.u.)	Speed ($\frac{mm}{s}$)	Repetition
5	1000	0.53 ± 0.01	5
10	1000	0.53 ± 0.01	5
30	1000	0.53 ± 0.01	5
100	1000	0.53 ± 0.01	1

In figure 3.20 an example of the 30 % strain cycle is plotted over time. The color code is used for the stress-strain curve to show the time dependence.

The three interesting parameters for the testing of the stretchable conductors are shown in figure 3.21. The starting resistance R_0 is the representation of the conductivity of the sample. The normalized resistance for the stretched state ($\frac{R}{R_0}$ Stretched) shows the change in resistance when stretched and the normalized resistance when relaxed ($\frac{R}{R_0}$ Relaxed) is a measure for the recovery of the resistance. The deviation of these two values is also a measure for the repeatability and reliability of the conductor.

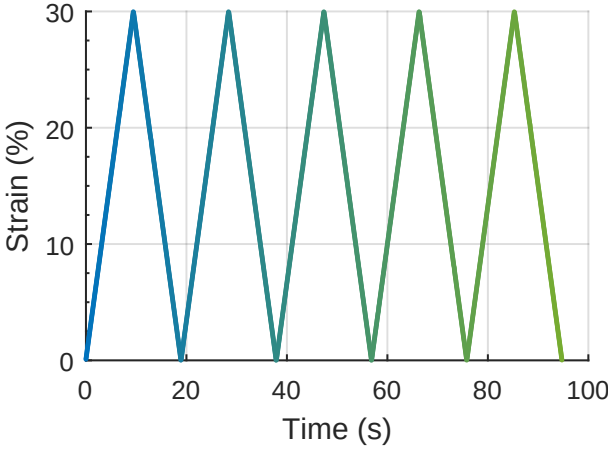

Figure 3.20.: Exemplary plot for the strain cycle of 30 %

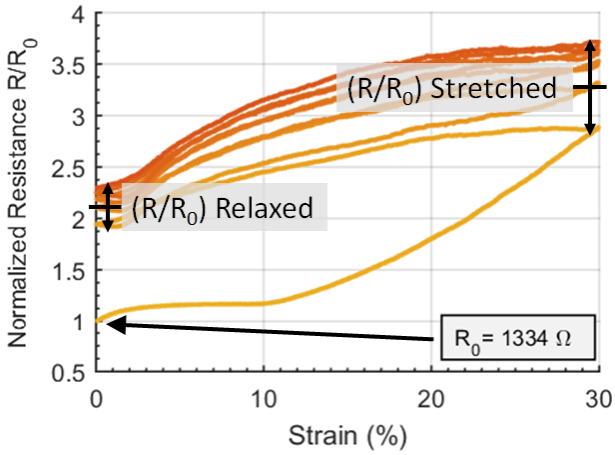

Figure 3.21.: Definition of interesting parameters for the stretchable conductors showing the starting resistance R_0, relative resistance $(\frac{R}{R_0})$for the stretched and relaxed state

3.4. Electrocardiography

The third main part of this thesis was to manufacture a working prototype of an ECG electrode based on the medical adhesive (MA-ECG electrode) for Umana Medical Technologies from Malta. As a stretchable conductor the IPC was chosen.

Although, the manufacturing process was part of the thesis it can not be explained, because it contains sensitive data and the intellectual property rights belong to Umana Medical Technologies.

In order to compare the ECG recording performance of the prototype with the commercially available Ag/AgCl electrode, the size of the active sensor area was made the same. The active area is a circle with a diameter of d = 15 mm as on the Ag/AgCl electrode.

3.4.1. Recording of ECG Signals

The ECG signals were recorded with an Arduino microcontroller and an ECG shield from Olimex. The first recordings were asynchronous which means that the signals from the two electrodes were not recorded at the same time. The latest measurements were done with two ECG shields at the same time and are synchronous which allows better comparison of the signals. The code for the recording with the Olimex ECG shield and the Arduino can be found in listing B.1 in the appendix.

The placement of the electrodes is very crucial for the signal which is obtained and is shown in figure 3.22. The electrode which was used as a reference is a standard disposable Ag/AgCl electrode from Covidien (H124SG). For the recording the electrodes were placed next to each other and the signal was recorded for some arbitrary amount of time.

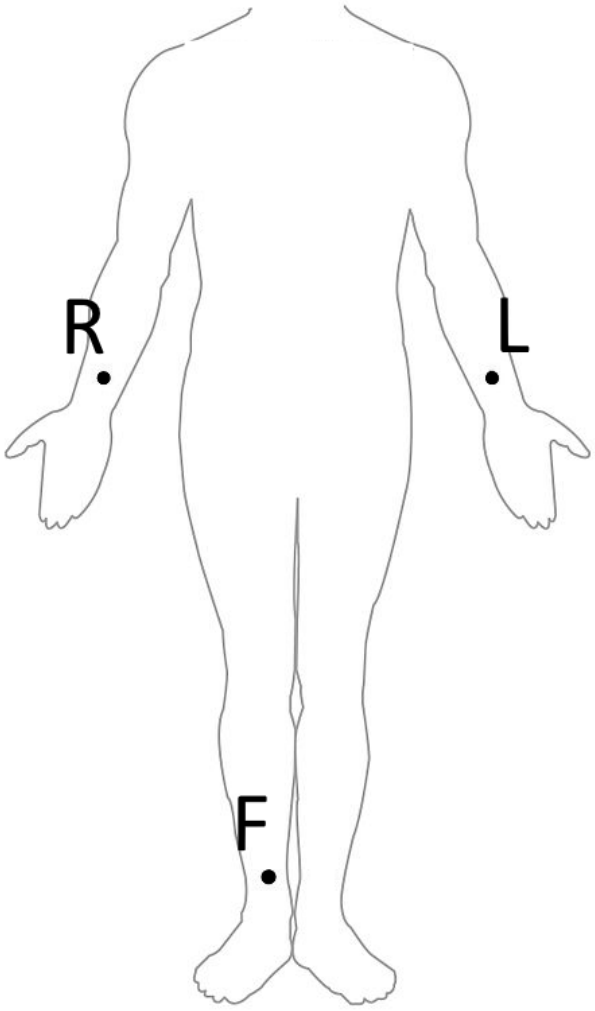

Figure 3.22.: Placement of electrodes for ECG recording

4. Experimental Results

In this section the results of the experiments explained before are shown. First, the characterization of the three conductive polymer inks (PEDOT:PSS) regarding thickness and conductivity are presented. Then, by the characterization of the laser induced carbon (LIC) regarding thickness and conductivity and the pictures taken with the scanning electron microscope to inspect the material morphology. Next, the results regarding calibration and verification of the electromechanical stretching setup are shown. Then, the outcome of the experiments for the characterization of the stretchable conductors are shown. Finally, the ECG recordings taken with the electrode prototype and a commercially available Ag/AgCl electrode can be found.

4.1. Characterization of Conductive Inks

For the characterization of the conductive inks the different inks were printed onto a glass substrate with different drop spacing (25, 35 and 45 µm) and number of layers (1,3 and 5). Then the sheet resistance and the thickness of the conductive polymer films were measured. With these values and equation (2.3) the conductivity for the different inks and the different printing parameters was calculated. This three values are shown in the following plots for films printed on a glass substrate because this made it possible to measure the film thickness.

4.1.1. Clevios™ P JET700

The plots in figure 4.1 show the results for the Clevios™ P JET700 ink.

The sheet resistance in figure 4.1a shows an increase with increasing drop spacing. This makes sense since the deposited film should get thinner and hence less conductive. The big value for 1 layer of PEDOT:PSS with a drop spacing of 45 µm is explained by a film which has a bad coverage resulting from the small volume of ink used to print it. As the number of layers increased the resistance got smaller and resulted from a thicker conductive film.

This is supported by the thickness plotted in figure 4.1b which shows a clear increase with increasing number of printed layers and a decrease with increasing drop spacing. A striking feature are the big error bars for a drop spacing of 35 µm for three and five layers. The error comes from a very rough surface (shown in figure B.1 in the appendix) of the printed film. Due to error propagation they are also present in the plots for the conductivity.

In figure 4.1c the conductivity shows the same behavior as the thickness. An increase of layers and a decrease of drop spacing result in an increasing conductivity. Although a slight saturation of the conductivity between three and five layers can be seen. The values for this number of layers are in good agreement with the specification of the manufacturer ($\sigma > 650\,\mathrm{S/cm}$).

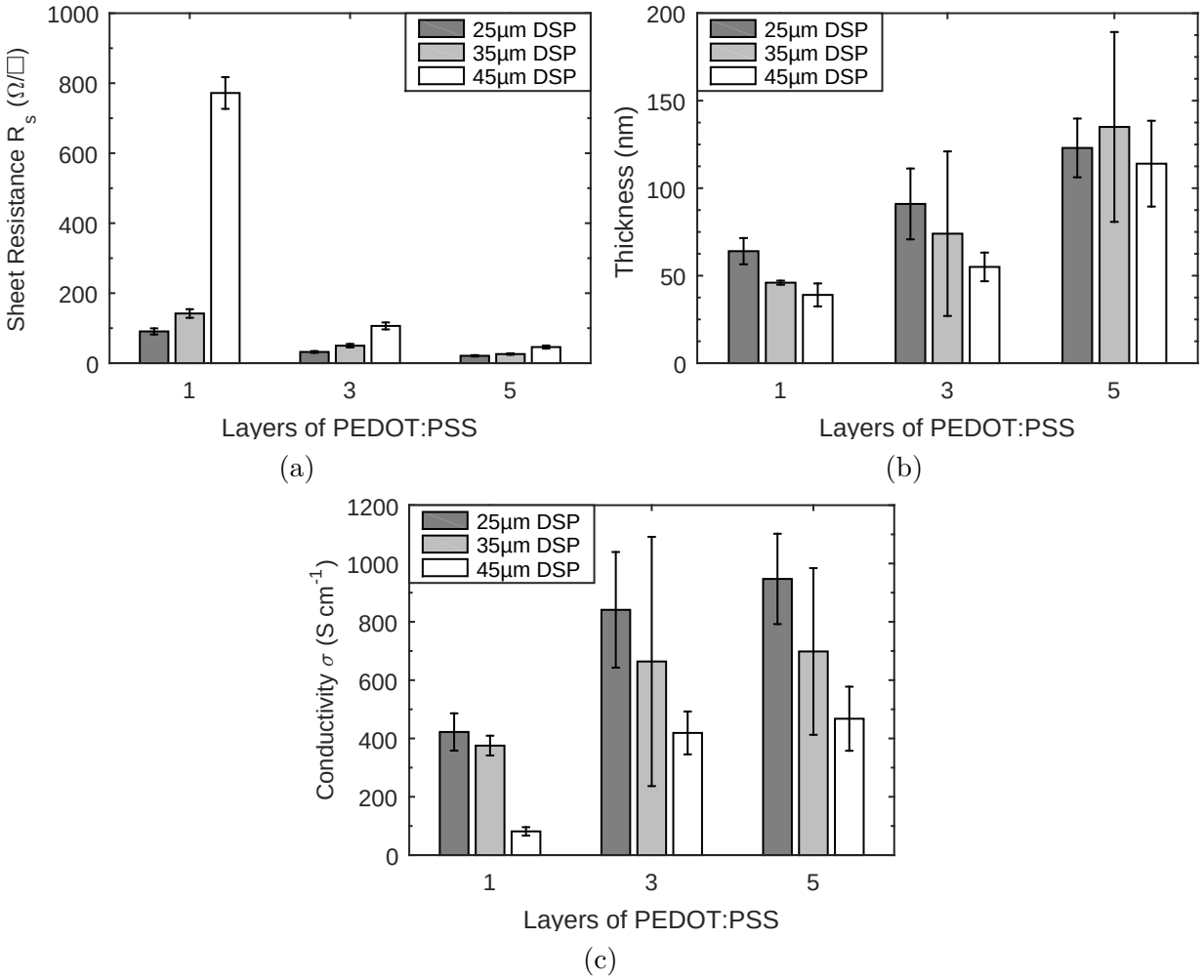

Figure 4.1.: Measurement results showing sheet resistance, thickness and conductivity over drop spacing and number of layers for the PJET700 ink

4.1.2. Clevios™ P JET700 N

The plots in figure 4.2 show the results for the Clevios™ P JET700 N ink.

The sheet resistance plotted in figure 4.2a shows a decrease with increasing number of printed layers and a decrease with increasing drop spacing. This is again because of the thickness of the film shown in figure 4.2b.

The thickness shows a clear increase with increasing number of printed layers and a decrease with increasing drop spacing. The only exception is the value for a drop spacing of 35 µm with five layers of printed PEDOT:PSS but this can be because of the big error from the measurement.

The conductivity values in figure 4.2 don't show anticipated behavior which would be a increase of conductivity with decreasing drop spacing. But this could be as a result of the big errors in the calculation. The conductivity increases with the number of layers as it should be and the values for the three and five layers again show a kind of saturation which is higher than the specified conductivity ($\sigma > 500\,\mathrm{S/cm}$). The big errors are again from the very rough surface and error propagation from the thickness measurement.

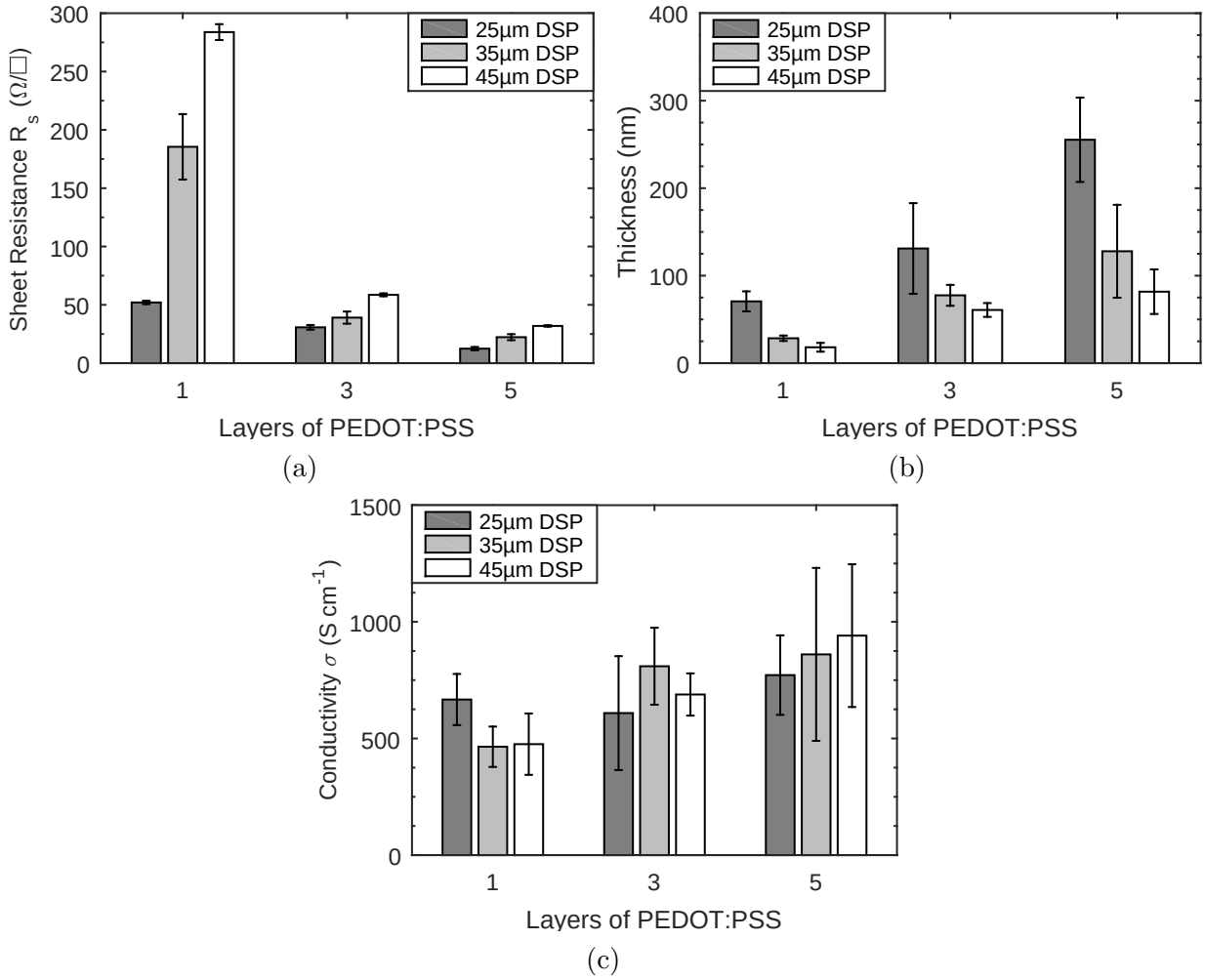

Figure 4.2.: Measurement results showing sheet resistance, thickness and conductivity over drop spacing and number of layers for the PJET700N ink

4.1.3. Comparison

To be able to compare the inks easier, section 4.1.3 shows all inks in one plot. The values are for a drop spacing of 35 µm and for 1, 3 and 5 layers. The ink with the highest conductivity is the Clevios™ P JET700 N, followed by the Clevios™ P JET700. Regarding the printability and the handling while and after printing the Clevios™ P JET700 N was also the best compared to the other two. The problem with the normal Clevios™ P JET700 is the clogging of the nozzles and destroying of the print head due to its low pH-value.

Since all these measurements were done on the glass substrate, some samples on the medical adhesive (MA) were made. With a drop spacing of 35 µm three layers of PEDOT:PSS were printed and the sheet resistance was measured. The thickness of the films was assumed to be the same as the ones on glass since the deposition volume did not change and it was not possible to measure the thickness with the profilometer on the adhesive side of the MA. Figure 4.4 shows the three inks and the conductivity for the film on glass and on the MA. For the inks from Clevios (P JET 700 and P JET 700N) the conductivity on the MA is smaller than on glass. The big error bars are once again from the very rough film surface.

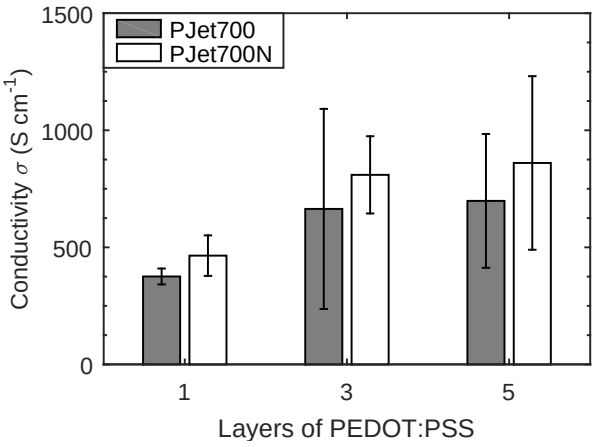

Figure 4.3.: A comparison of conductivity between the different conductive polymer inks printed with a drop spacing of 35 µm for 1, 3 and 5 layers

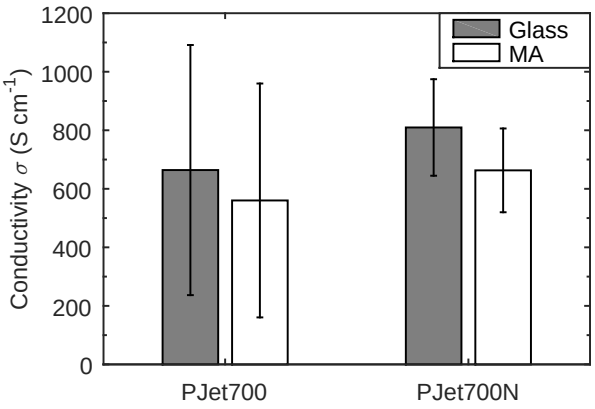

Figure 4.4.: A comparison of the conductivity of all inks between the films on glass and on the medical adhesive (MA) printed with a drop spacing of 35 µm and 3 layers (thicknesses were assumed to be the same in both cases)

4.2. Laser Induced Carbonization

The laser induced carbon used for the LICC were also characterized regarding thickness and conductivity. Whereas the thickness for the LIC-Fiber film was impossible to measure due to its morphology and the length of the fibers was only estimated with the help of the SEM pictures. The morphology of the films was investigated with a SEM and the pictures are shown in the last part of this section.

4.2.1. Characterization of Laser Induced Carbon

The characterization for LIC was only be done for LIC-Flat. This was because the thickness for LIC-Fiber was not possible to measure and the sheet resistance was more or less impossible to measure because of the 3D structure of the fibers (see figure 4.6). So in figure 4.5 the sheet resistance and conductivity for the LIC-Flat film with a thickness of 8.7 ± 1.4 µm is shown. The sheet resistance for the transferred sample is around ten times higher than the resistance of the sample in the original PI substrate. This can also be seen in the conductivity plot where the conductivity is also different by a factor of 10. The lower conductivity could be caused by the transfer and destruction of the porous carbon structure.

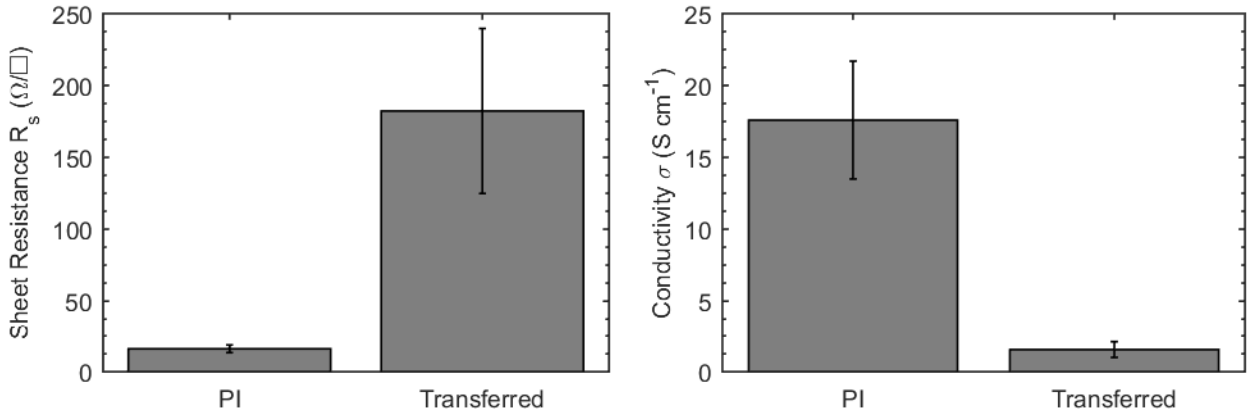

(a) (b)

Figure 4.5.: Measurement results showing sheet resistance, conductivity for LIC with a thickness of $8.7 \pm 1.4\,\mu m$ in carbon and transferred onto the medical adhesive

4.2.2. Morphology of Laser Induced Carbon

In this section the morphology of the laser induced carbon is investigated with the help of pictures taken with a scanning electron microscope. In figure 4.6 the two different power settings for the LIC are shown, in the left column the LIC-Flat (Power = 10 %) is shown. In the right column the power setting (Power = 20 %) where macroscopic fibers are produced is shown.

The first row shows the pictographs of the two LIC forms (left = LIC-Flat, right LIC-Fiber).

The second row shows a picture of the surface with a magnification of 150 for both surfaces. The LIC-Flat (left, (a)) shows a very flat surface with trenches from the laser and a few brighter highlights on the edges of this trenches. Compared to this the LIC-Fiber (right, (b)) shows a completely different surface structure with big cones emerging from the surface. This cones have a length of 100 to 200 µm and are densely packed. Also the cones seem to have a preferential direction which could be because of the production method.

The third row shows a higher magnification of 650 times and highlights interesting areas. For the LIC-Flat (left, (c)) the trench was chosen, and one can clearly see the trench and the bulk. This looks like a very porous bulk which would be in agreement with the results stated in [10] where they talk about porous graphene. Unfortunately, there was no more time left to investigate the composition of the produced material with Raman Spectroscopy and look for graphene peaks. And this is the reason why in this thesis only the word laser induced carbon and not laser induced graphene (LIG) is used. On the right side (d) a single cone consisting of many smaller fibers is shown. So, the macroscopic fibers are made up of many microscopic fibers of the same length but with a much smaller diameter.

In the last row some features are magnified even more and for the LIC-Fiber (left, (e)) the bright features next to the trenches were chosen. The picture shows that the bright areas are very small fibers with a few micrometers in size. So even the LIC-Flat has small carbon fibers emerging from the porous carbon bulk. For the LIC-Fiber (right, (f)) a section of the cone was magnified, and it shows that the fibers have a diameter of a few hundred micrometers.

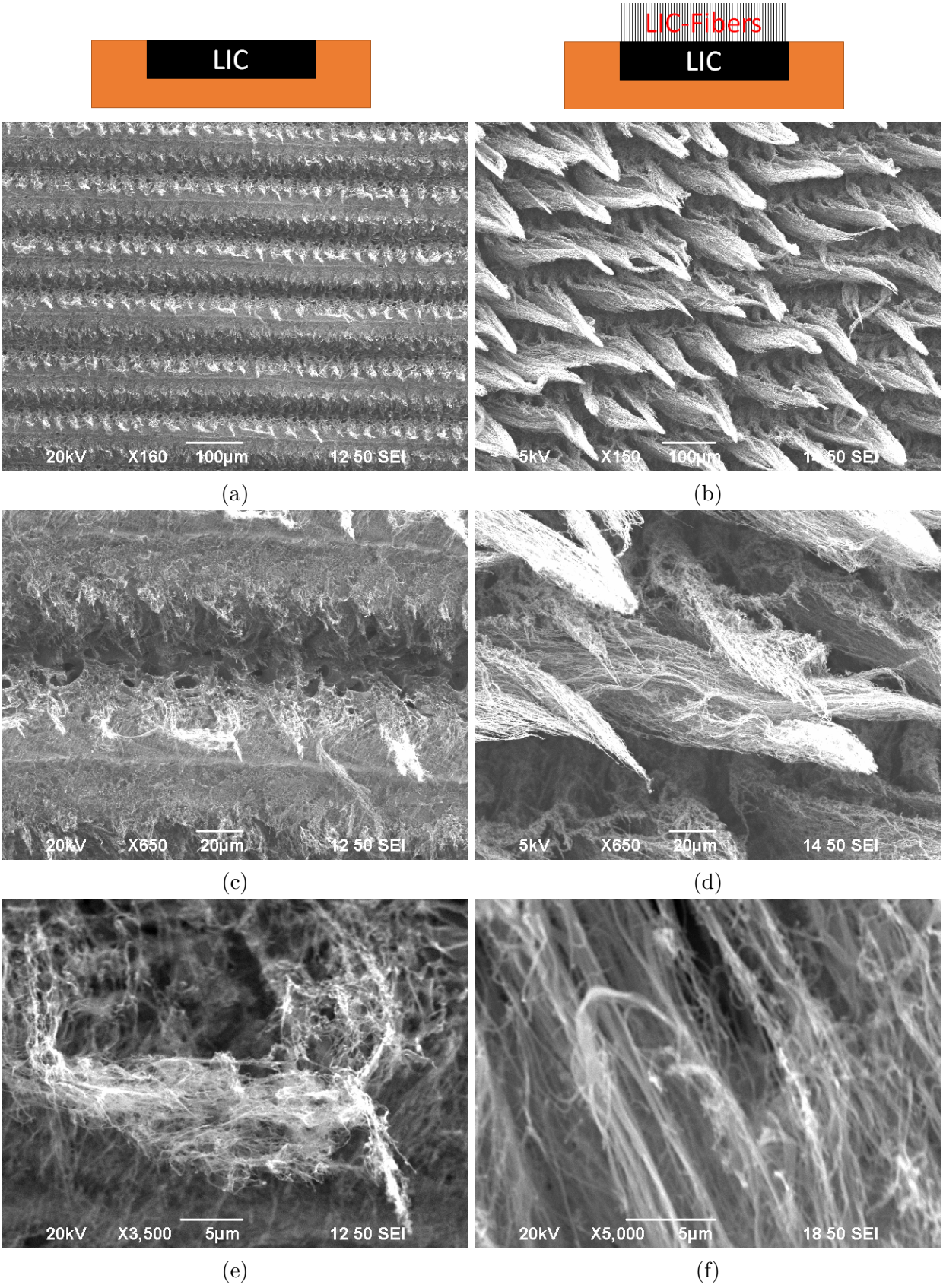

Figure 4.6.: Morphology of the top surface of the carbon film produced with laser induced carbonization for LIC-Flat (left column) and LIC-Fiber (right column)

Up to now only the top surface of the LIC was investigated, to get a better idea of the bulk the carbon was transferred (shown in figure 3.8) to the medical adhesive and so the bottom of the LIC could be investigated. The first row in figure 4.7b shows the pictograph of the investigated sample. Note that now the top surface of the sample is now the bottom of the LIC bulk produced in the polyimide.
In figure (a) the surface is shown with a magnification of 150 times and shows a flat surface with a few ridges which come from the laser. Enhancing the magnification to 650 times one can identify single flakes of carbon which make up the bulk. With an even higher magnification of 7800 times the carbon flakes are shown more clearly and since they are shown as semitransparent they seem to be very thin. Again, the porous structure can be seen in this picture.

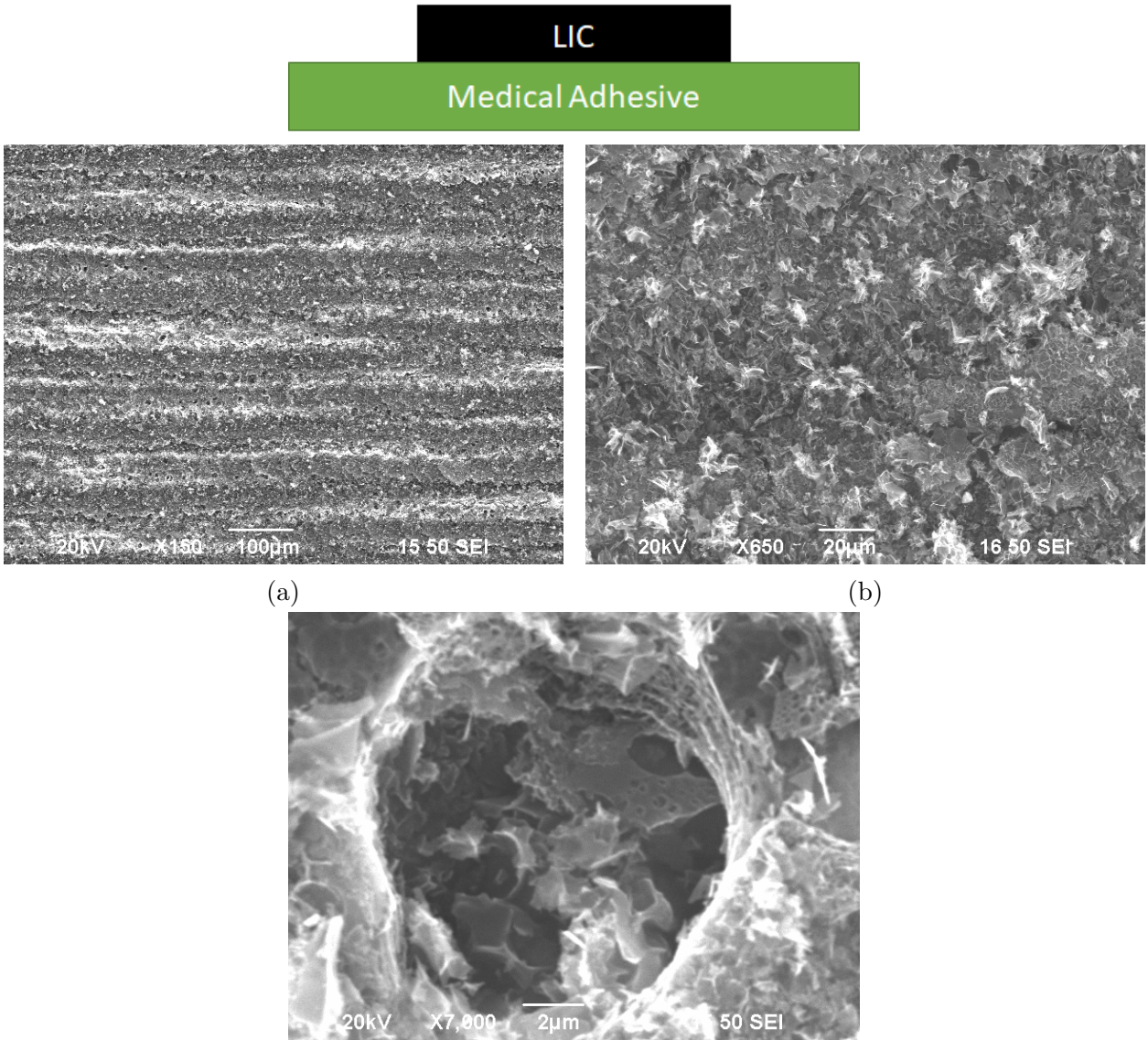

(a) (b)

(c)

Figure 4.7.: Morphology of the bottom surface of the carbon film produced with laser induced carbonization which was transferred onto the medical adhesive to make it accessible

The same as the transfer for the LIC-Flat was done for the LIC-Fiber (also shown in figure 3.8) to investigate the transferred fibers. In figure 4.8 the first row again shows the

pictograph of the investigated sample. In figure (a) the transferred fibers are shown with a magnification of 150 times. It shows that the orientation of the fibers is gone and that the fibers seem to be broken or bent.
A magnification of 650 times is shown in figure (b), there the single fibers can be identified again. Also, the white spots in the top of the figure show the underlying medical adhesive which is white due to electrical charging.

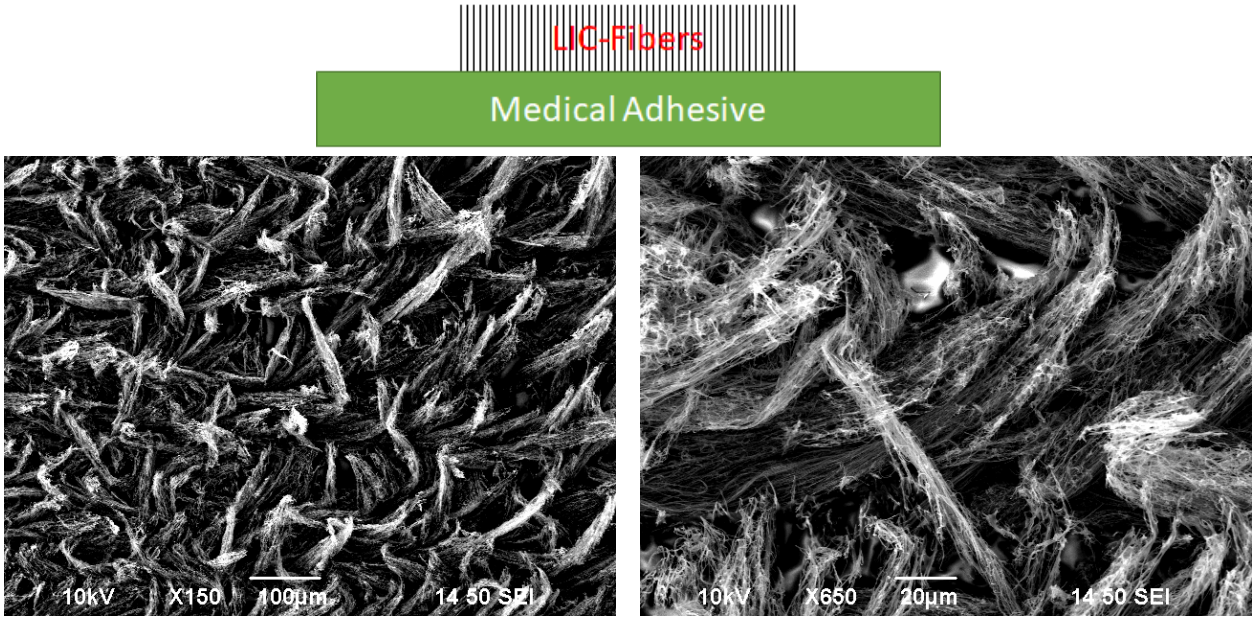

(a) (b)

Figure 4.8.: Morphology of the transferred LIC-Fiber produced with laser induced carbonization which was transferred onto the medical adhesive

4.3. Electromechanical Stretching Setup

This section is about the calibration and verification of the electromechanical stretching setup. The calibration and verification was done by Michael Gobald in his bachelors thesis. The determination of the speed in $\frac{mm}{s}$ was done together and can be found after the calibration section.

4.3.1. Calibration of the Load Cell

The calibration of the load cell was done by Michael Gobald as a part of his bachelors thesis [15]. As explained before a pulley was used to direct the force of known weights to the load cell. Since the defined measurements use the load cell only in extension mode this is sufficient. The weights used for the calibration were 0, 14.37, 56.6, 86.15 and 113.4 g. The maximum weight was defined by the maximum load of the load cell (0.25 lb = 113.4 g). The microcontroller has a analog-digital convert (ADC) with 1024 bits and a range of 0 to 5 V. This gives a accuracy of 4.9 mV/bit for the conversion. The maximum load of 113.4 g should correspond to a output voltage of 5 V and this gives a conversion error of 0.1 g.
The values (now as force (N)) shown in figure 4.9 were measured by Michael at different stages in his thesis to get values for the drift of the calibration. The linear fits shows a very

good agreement with the data points but has a slight zero shift of 0.3×10^{-3} N, which is smaller than the conversion error. However, at the upper limit the values deviate from the applied force (see table 4.1) which could be due to a combination of zero shift and a poor gain value. For our purposes this was enough to start measurements, but for high precision measurements the calibration should be redone with a better gain setting.

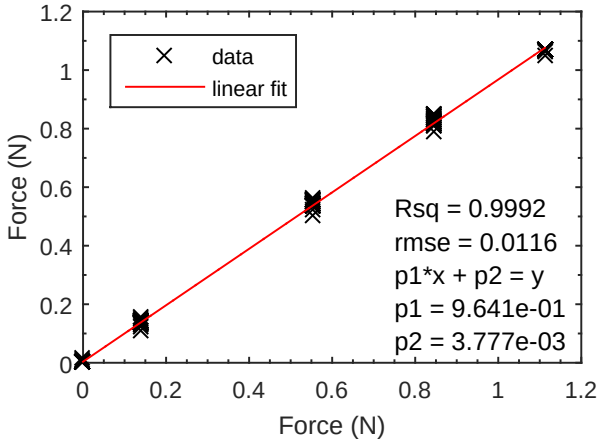

Figure 4.9.: Calibration curve for the load cell

Table 4.1.: Weights used for calibration and their measured values in grams

Applied Weight (g)	Measured Weight (g)
0.00	0.00 ± 0.31
14.37	14.06 ± 0.98
56.60	55.13 ± 1.39
86.15	84.23 ± 1.67
113.40	108.94 ± 0.52

4.3.2. Determination of Speed

To determine the real speed of the setup a small python script was written. This script sends a command to move the stage with a specified speed (a.u.) to a certain position and measures the time it takes to arrive there. Knowing the traveled distance and time, it is possible to calculate the speed in $\frac{\text{mm}}{\text{s}}$. The measurements shown in figure 4.10 show a linear behavior up to a speed of 12 000 a.u. were the values get constant. This upper limit of the speed is determined by the clock speed of the microcontroller and the screw pitch of the stage. The variation of the values starting with 12 000 a.u. is from acceleration and deceleration when using different distances to measure the speed. So a theoretical maximum speed of $6.38 \pm 0.08 \frac{\text{mm}}{\text{s}}$ could be reached. However, the realistic maximum speed is limited by the number of steps per data point. If the speed and the steps per data point are high than very little data points are gather per measurement and a lot of information is lost. At the moment the bottle neck is the measurement speed of the Keithley source meter for the resistance measurement. The time it takes to make one measurement is around 30 µs, that limits the realistic maximum speed to around $0.5 \frac{\text{mm}}{\text{s}}$. The conversion of some common arbitrary units to $\frac{\text{mm}}{\text{s}}$ can be found in table 4.2. For a higher speed a better solution for the resistance measurement has to be found, more about this in *Appendix A Room for Improvements*.

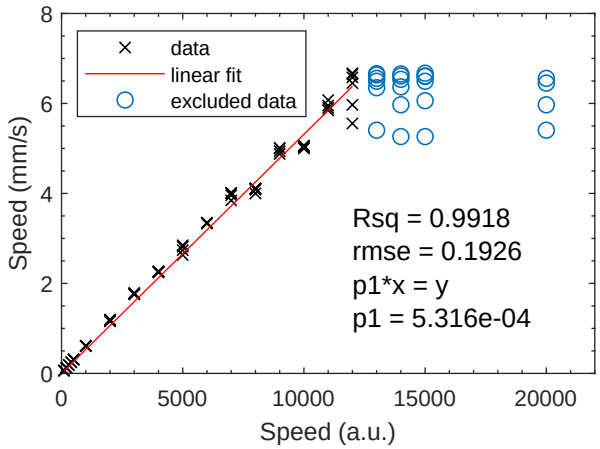

Figure 4.10.: Measurement curve for the determination of the speed in $\frac{mm}{s}$, linear up to a speed of 12 000 a.u. = 6.4 $\frac{\text{mm}}{\text{s}}$

Table 4.2.: Conversion of common speed values form arbitrary units in $\frac{mm}{s}$

Speed (a.u)	Speed ($\frac{mm}{s}$)
500	0.27 ± 0.01
1000	0.53 ± 0.01
2000	1.06 ± 0.01
5000	2.66 ± 0.03
10 000	5.32 ± 0.07
12 000	6.38 ± 0.08

4.3.3. Verification

For the verification of the setup a known crosslinked silicon rubber called Elastosil® was used by Michael Gobald. This material is produced by Wacker Chemie AG and a tensile measurement is provided on their homepage (see figure 4.11a) [16]. The material had a thickness of 20 µm and was cut into stripes for the measurement. Here just a quick glance is given onto one of the measurement curves done by Michael Gobald which is shown in figure 4.11b. The curve has a good agreement with the reference measurement and shows a similar form. For more details and measurements of other reference materials such as polydimethylsiloxane (PDMS) please take a look at the bachelor thesis of Michael Gobald [15].

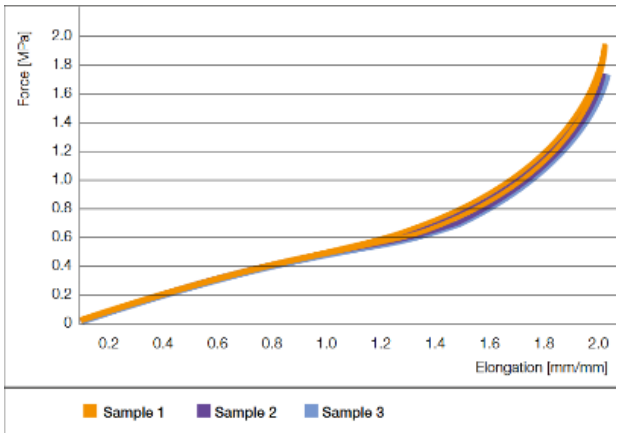

(a) Tensile test of Elastosil® provided by Wacker Chemie AG on their homepage [16]

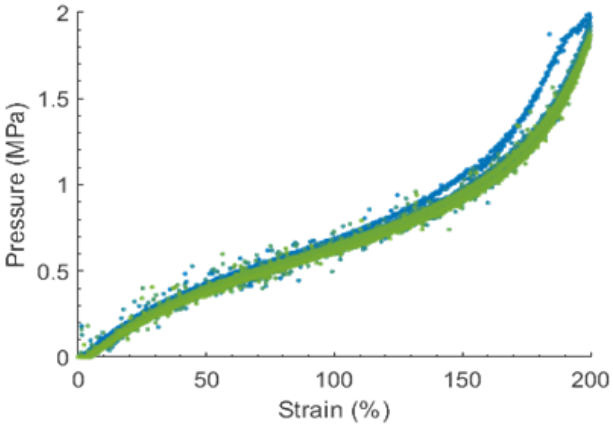

(b) Tensile test of Elastosil® done with the electromechanical stretching setup

Figure 4.11.: Comparison of tensile test of Elastosil® done by Wacker Chemie AG and Michael Gobald

4.4. Stretchable Conductors

This section is about the testing of the different stretchable conductors. First the mechanical properties of the medical adhesive are investigated and then the electromechanical properties of the stretchable conductors are shown. At first the results for the IPC and then the results for the LICC are shown. At the end a composite conductor, a combined of both (laser induced carbon fibers with PEDOT:PSS printed on top) is shown.

4.4.1. Medical Adhesive

The stress-strain curves for the medical adhesive are discussed in this section. Since the conductors did not have any influence on the mechanical properties of the medical adhesive, these are examined separately.

In figure 4.12 the four strain cycles (5, 10, 30 and 100 %) are shown. Each cycle was performed with the same sample, so the imposed deformation of the leading cycle has an influence on the measurement. But since the main focus was the electromechanical behavior this presents no real problem.

The plotted curve for 5 % strain (figure 4.12a) shows a very linear behavior and nearly no loss which speaks for a elastic behavior. For a strain of 10 % (figure 4.12b) a very small hysteresis can be spotted and marks the end of the elastic region. The loss in figure 4.12c is the biggest for the first cycle and gets smaller for the other four. This phenomena is called cyclic softening and is typical for thermoplastic polyurethane ([17]). The plot figure 4.12d shows the 100 % strain cycle and shows a very plastic behavior.

The Young's modulus calculated with equation (2.1) was 15 ± 5 MPa. The value is the Young's modulus taken at the beginning of each cycle since this value is strain and cycle dependent.

For all cycles the loss was calculated according to equation (2.2) and is shown in table 4.3. The loss for the first cycle (Loss C1) increased form a value of 0.24 to 0.45 and the mean of the cycle two to five (Loss C2-C5) stayed around 0.20. The difference of this two values ($Delta$Loss) shows the difference caused by the cyclic softening.

The remaining plastic deformation off all cycles is shown in table 4.4 and shows that one can apply a rule of thumb that the plastic deformation is a tenth of the imposed strain.

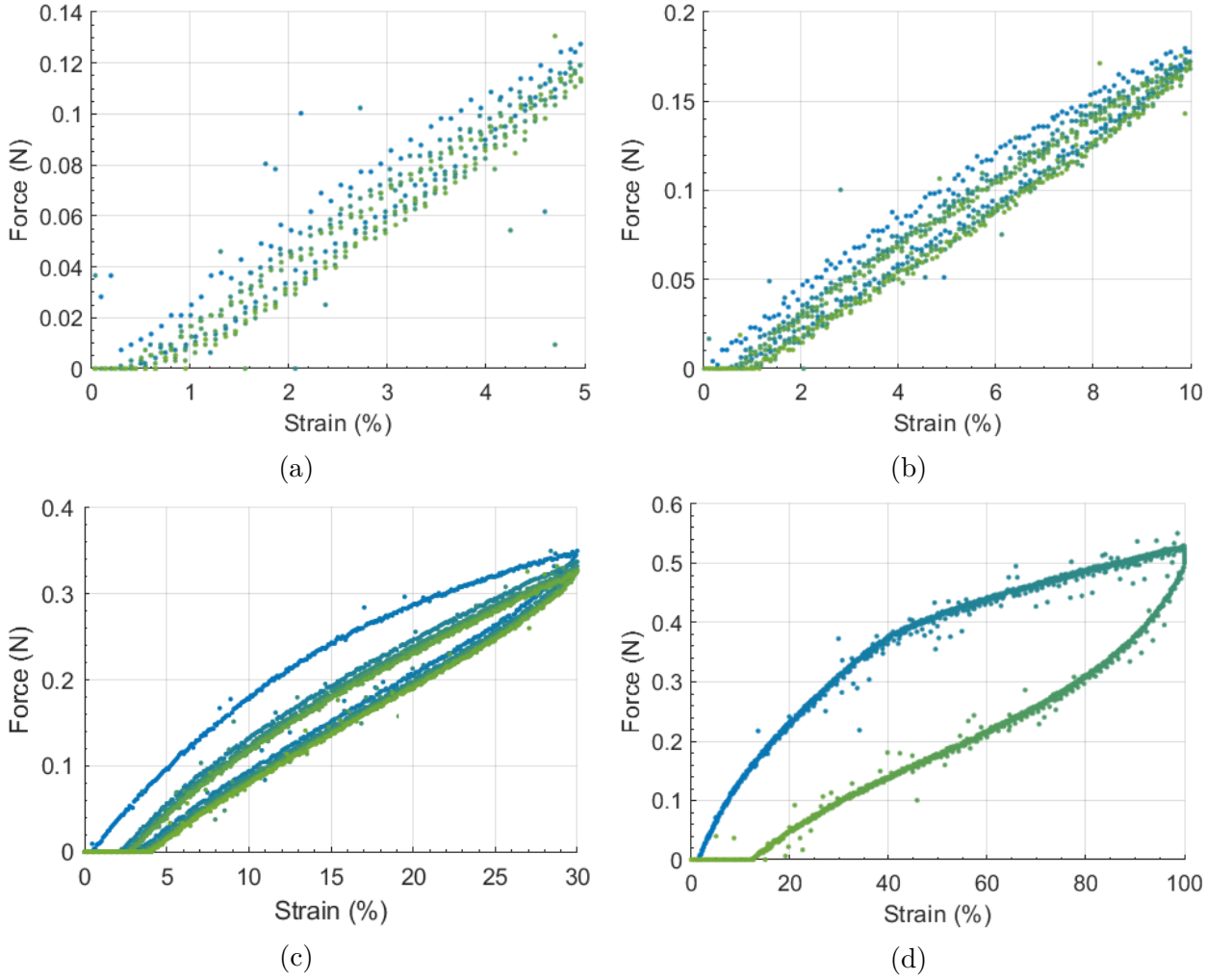

Figure 4.12.: Stress-strain plots for the four strain cycles showing plastic deformation and cyclic softening

Table 4.3.: Energy loss due to plastic deformation and heat dissipation according to equation (2.2)

Strain (%)	Loss C1	Loss C2-C5	ΔLoss
5	0.24 ± 0.03	0.21 ± 0.03	0.04
10	0.24 ± 0.02	0.18 ± 0.01	0.06
30	0.31 ± 0.01	0.20 ± 0.01	0.11
100	0.45 ± 0.01		

Table 4.4.: Remaining plastic deformation after stretching and relaxing

Strain (%)	Plastic Deformation (%)
5	0.32 ± 0.04
10	0.63 ± 0.10
30	2.23 ± 0.14
100	13.16 ± 0.34

4.4.2. Ink-jet Printed Conductors

For the ink-jet printed conductors (IPC) three layers of PEDOT:PSS with a drop spacing of 35 µm were printed onto the stripes of medical adhesive. For this the two Clevios^{TM} inks (PJET700 and PJET700N) were used.

The plots in figure 4.13 show the strain cycle (5 %) and the change of the normalized resistance ($\frac{R}{R_0}$) over time in figure 4.13a. In figure 4.13b the normalized resistance is plotted over strain. The plots are color coded for a better understanding of the resistance change over time in figure 4.13b. At the start the data points are yellow and change their color with time to red. This is true for all future plots which show the change of normalized resistance over strain.

Figure 4.13a shows a very bad behavior for a stretchable conductor, with every cycle the resistance increases until it will eventually break. This behavior is also clearly visible in the plot over strain (figure 4.13b) where the starting resistance of 1877 Ω increase to a value of 2.5 times the original value.

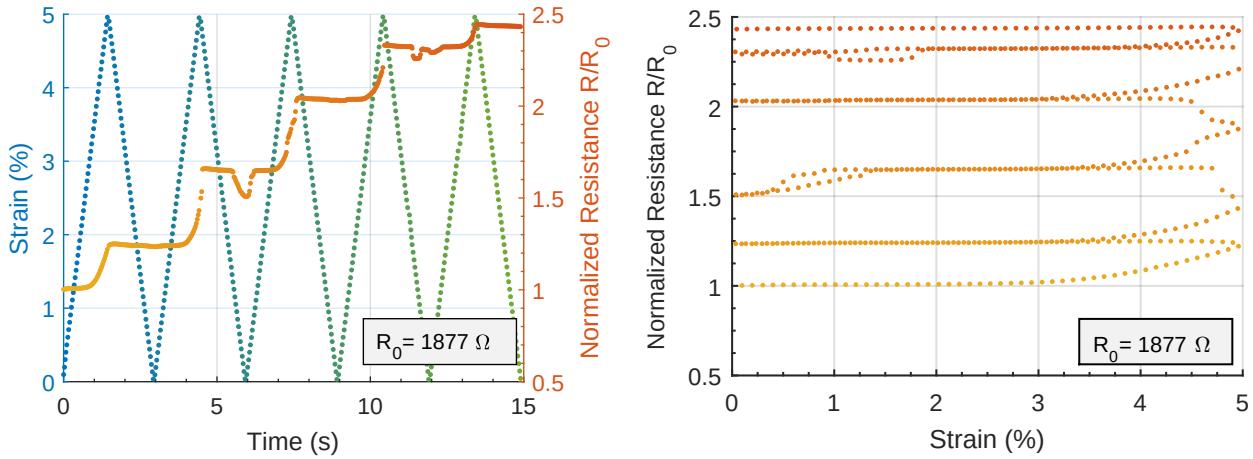

(a) (b)

Figure 4.13.: Exemplary strain cycle over time and relative resistance change ($\frac{R}{R_0}$) over time and strain of one IPC

The behavior observed in figure 4.13 can explained with figure 4.14. The not stretched state is shown in figure 4.14a and only a few small cracks from the drying and mounting process are visible. Compared to figure 4.14b where the sample was stretched a few percent a lot of cracks are visible. These cracks are responsible for the increase of resistance and with more cycles the cracks get more and bigger. This can be repeated until there are so many cracks so that the sample is not conductive anymore.

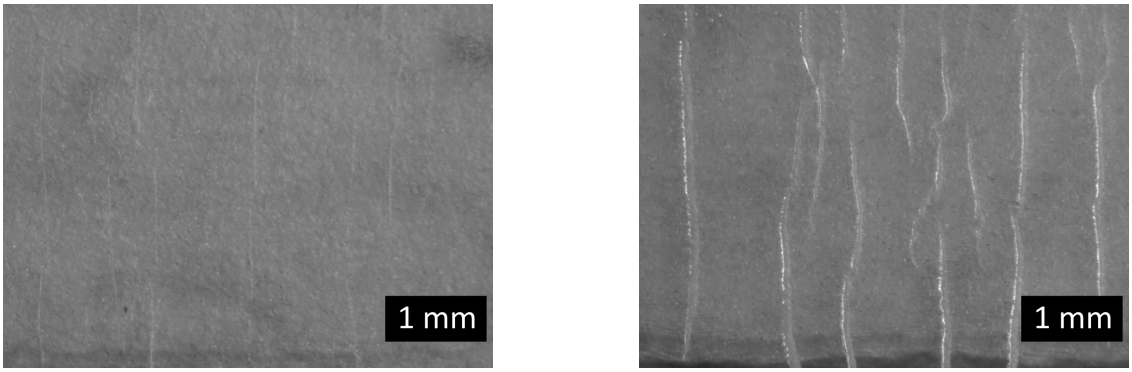

(a) not stretch (b) stretched

Figure 4.14.: Pictures of one IPC showing its not stretched and stretched state taken with a microscope

The plots shown so far were only a very good example of the IPC and were mainly used to explain the resistance change with the formation of cracks. In figure 4.15 two more plots of the IPC are shown. There a sample were the cracks are closed again after relaxation (figure 4.15a) and one where the sample breaks at the fourth stretching cycle (figure 4.15b).

The results from all samples were used to make a statistic for the three interesting parameters defined in section 3.3.3 (see figure 3.21).

In table 4.5 the values for PJET700 are shown for a stretching cycle of 5 % and 10 %. The resistance R_0 for PJET700 was $1.5 \pm 0.7\,k\Omega$ and the resistance for the stretched state at 5 % was $1.9 \pm 0.6\,R_0$. The relaxed state had a similar value of $1.7 \pm 0.5\,R_0$, which means that this conductor is not stretchable since the resistance tends to increase with every cycle without going back to the starting value. The same behavior can be observed for a stretching cycle of 10 % strain where the stretched and relaxed resistance where both around $7.0 \pm 0.5\,R_0$.

For the second ink PJET700N the values can be found in table 4.6 where only a stretching cycle of 5 % is listed. This is because this samples never survived a cycle of ten percent and this can also be seen in the table. In comparison to the PJET700 the starting resistance R_0 with a value of $800 \pm 600\,\Omega$ is much smaller than the one for PJET700N which confirms the better conductivity of PJET700 found in section 4.1.3. But the values for the stretched and relaxed state ($6 \pm 3\,R_0$) are much higher which means that this is much worse in regards to stretchability.

It has to be noted that there were samples of both inks which already broke at a strain of 2 % which is just a confirmation for the very bad and unreliable stretchability of the IPC.

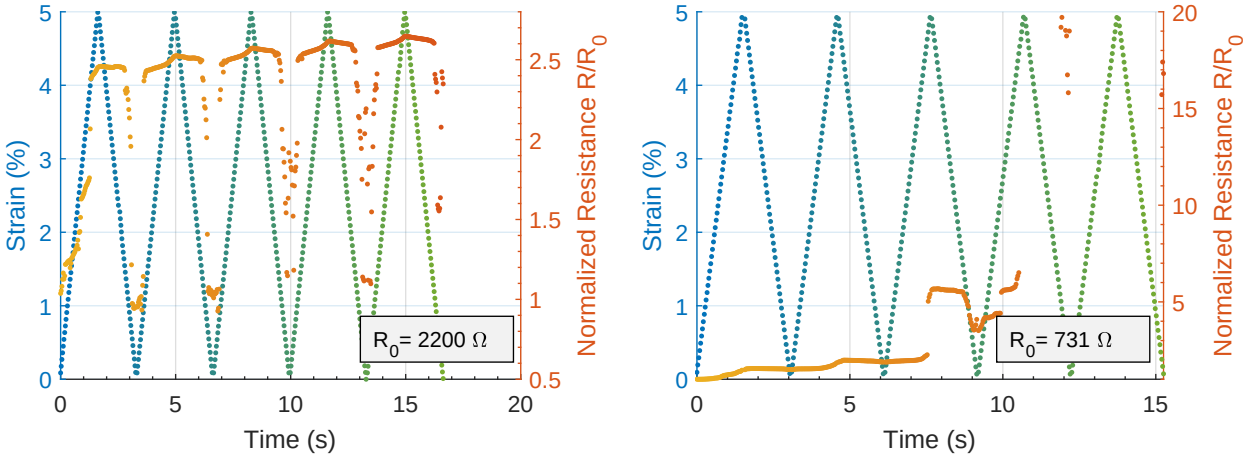

(a) (b)

Figure 4.15.: Exemplary strain cycle and relative resistance change ($\frac{R}{R_0}$) over time of two very bad IPC

Table 4.5.: Statistical results of the PJET700 conductor for different stretching cycles with R_0 the starting resistance and the relative resistance $\frac{R}{R_0}$ for the stretched and relaxed state

Strain (%)	R_0 (kΩ)	R/R_0 Stretched	R/R_0 Relaxed
5	1.5 ± 0.7	1.9 ± 0.6	1.7 ± 0.5
10	2.8 ± 1.3	7.1 ± 2.5	7.0 ± 2.5

Table 4.6.: Statistical results of the PJET700N conductor for different stretching cycles with R_0 the starting resistance and the relative resistance $\frac{R}{R_0}$ for the stretched and relaxed state

Strain (%)	R_0 (Ω)	R/R_0 Stretched	R/R_0 Relaxed
5	800 ± 600	6.1 ± 3.5	5.9 ± 3.2

4.4.3. Laser Induced Carbon Conductors

The laser induced carbon conductors (LICC) were tested in three variations. Two variations of LIC-Flat, namely LIC-Flate ∥ and LIC-Flat ⊥ and the LIC-Fiber all transferred onto the medical adhesive.

LIC-Flat ∥

For the LICC which were produced parallel to the stretching direction called LIC-Flat ∥ an exemplary stretching cycle of 30 % is shown in figure 4.16. The starting resistance R_0 is small with a value of around 1 kΩ and the conductor is stretchable up to a strain of 30 %. The resistance of the stretched state is increased with each cycle up to a value of over 20 R_0. Although the stretched resistance is very high, the resistance in the relaxed state goes almost back to the starting value (around 1.5 R_0).

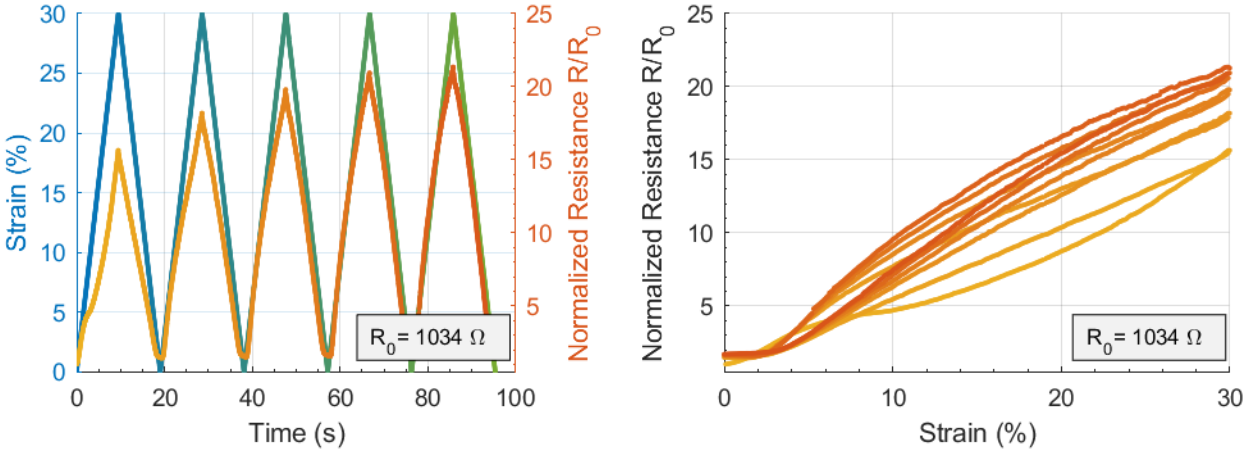

(a) (b)

Figure 4.16.: Exemplary strain cycle over time and relative resistance change ($\frac{R}{R_0}$) over time and strain of one LICC (LIC-Flat ||)

Again pictures of the not stretched and stretched state are shown in figure 4.17. The not stretched state in figure 4.17a shows the alignment of the carbon parallel to the stretching direction (horizontal), whereas figure 4.17b shows the stretched state. Here the formation of cracks and small carbon islands can be observed.

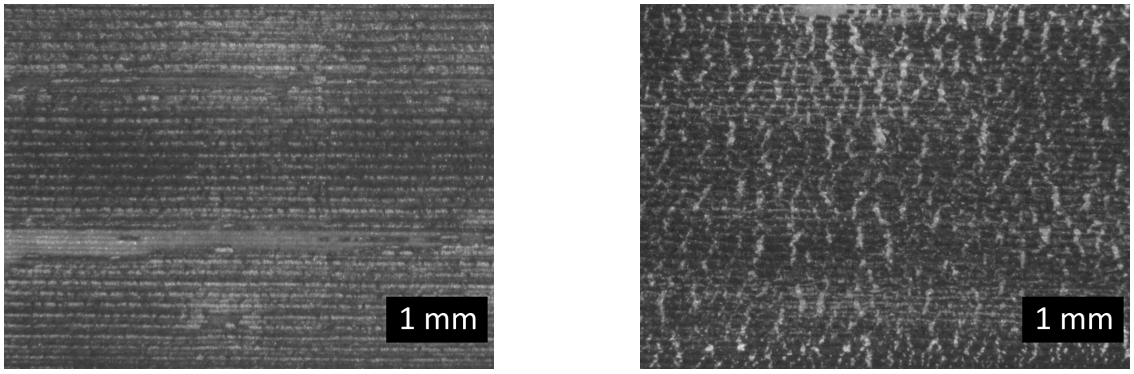

(a) not stretched (b) stretched

Figure 4.17.: Pictures of one LICC (LIC-Flat ||) showing its not stretched and stretched state taken with a microscope

Again the values of all samples measured were used to make the statistic in table 4.7. The table clearly shows that this LICC is a good stretchable conductor with a R_0 of around 1 kΩ. It gets to very high resistances with high strain values (at a strain of 30 % the resistance is $21 \pm 4\,R_0$) but also recovers to a value of around $1.6\,R_0$. In the row with a strain of 100 % it is shown that some samples broke at around 32 % of strain but also recovered back to a value of $3.5\,R_0$.

Table 4.7.: Statistical results of the LIC-Flat ∥ conductor for different stretching cycles with R_0 the starting resistance and the relative resistance $\frac{R}{R_0}$ for the stretched and relaxed state

Strain (%)	R_0 (Ω)	R/R_0 Stretched	R/R_0 Relaxed
5	930 ± 130	2.5 ± 0.2	1.09 ± 0.01
10	940 ± 130	4.5 ± 0.4	1.16 ± 0.02
30	990 ± 130	21 ± 4	1.64 ± 0.11
100	1200 ± 130	broken at 32%	3.54 ± 0.06

LIC-Flat ⊥

For the LICC produced perpendicular to the stretching direction called LIC-Flat ⊥ an exemplary plot is shown in figure 4.18. The starting resistance (R_0= 3.5 kΩ) is higher compared to its parallel counterpart but the relative resistance change for the 30 % strain cycle is smaller with a value of around 15 R_0. The resistance at the relaxed state is around 1.5 R_0 and shows a very good stretchability.

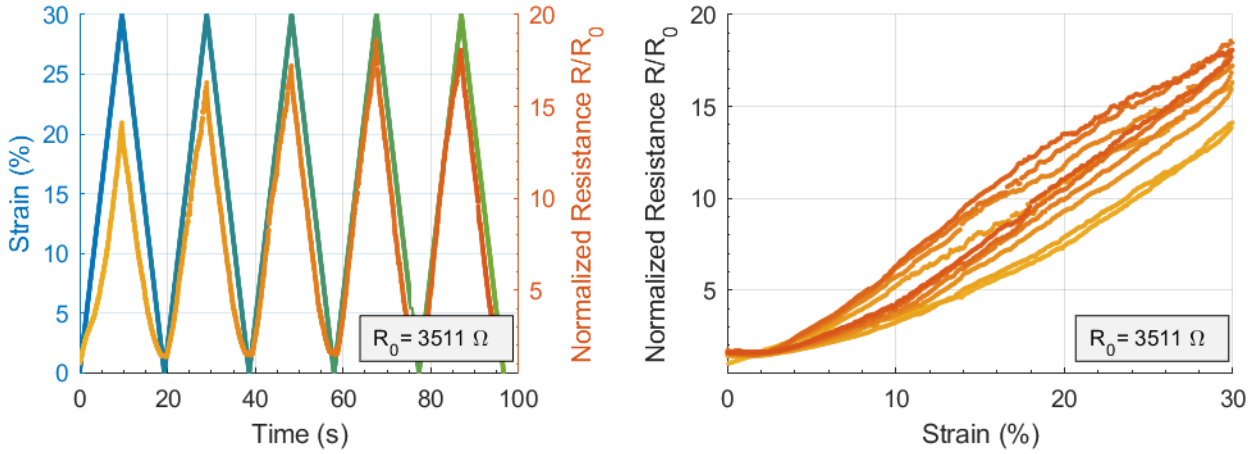

(a) (b)

Figure 4.18.: Exemplary strain cycle over time and relative resistance change ($\frac{R}{R_0}$) over time and strain of one LICC (LIC-Flat ⊥)

The pictures for the not stretched state in figure 4.19a shows the alignment of the carbon perpendicular to the stretching direction (horizontal). In the stretched state (figure 4.19b) one can see the formation of pockets surrounded by carbon.

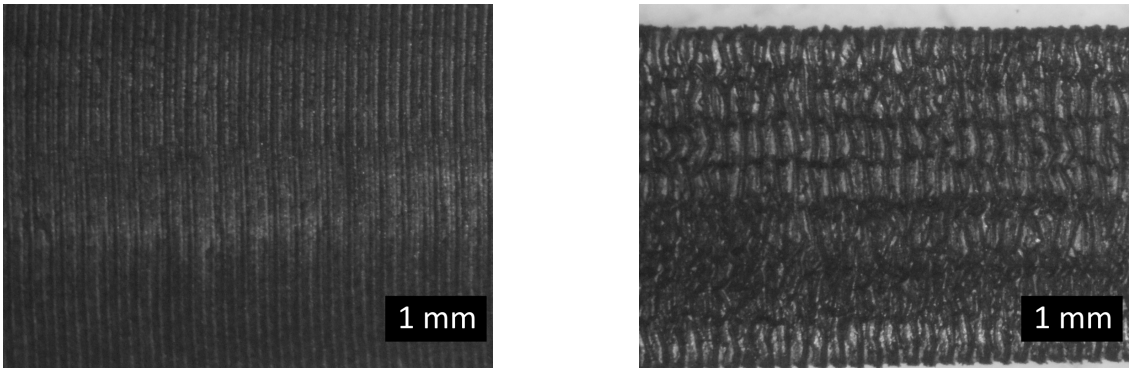

(a) not stretched (b) stretched

Figure 4.19.: Pictures of one LICC (LIC-Flat ⊥) showing its not stretched and stretched state taken with a microscope

The statistical results in table 4.8 show a higher starting resistance R_0 of 3 kΩ. But it also shows that it is a very good stretchable conductor which can be stretched over 30 % and recovers to a value of 1.5 R_0 after stretching. Even after a stretching to 100 % where the sample breaks, it has a resistance of only 2.5 R_0 after recovering.

Table 4.8.: Statistical results of the LIC-Flat ⊥ conductor for different stretching cycles with R_0 the starting resistance and the relative resistance $\frac{R}{R_0}$ for the stretched and relaxed state

Strain (%)	R_0 (kΩ)	R/R_0 Stretched	R/R_0 Relaxed
5	3.1 ± 0.2	1.8 ± 0.2	1.14 ± 0.02
10	3.2 ± 0.2	2.7 ± 0.5	1.17 ± 0.01
30	3.4 ± 0.2	12 ± 4	1.52 ± 0.10
100	4.5 ± 0.3	broken at 38%	2.5 ± 0.7

LIC-Fiber

For the LICC produced from transferred LIC-Fibers onto medical adhesive an exemplary plot for a stretching cycle of 30 % is shown in figure 4.20. The starting resistance R_0 is very high with a value of around 10 kΩ. The plot for normalized resistance versus strain in figure 4.20a shows an interesting behavior compared to the conductors tested so far. After the first cycle it seems that the stretchable conductor reaches a kind of stable state where the resistance for the stretched state is around 3 R_0 and for the relaxed state around 1.5 R_0. This behavior was not seen before with other stretchable conductors and is a good behavior.

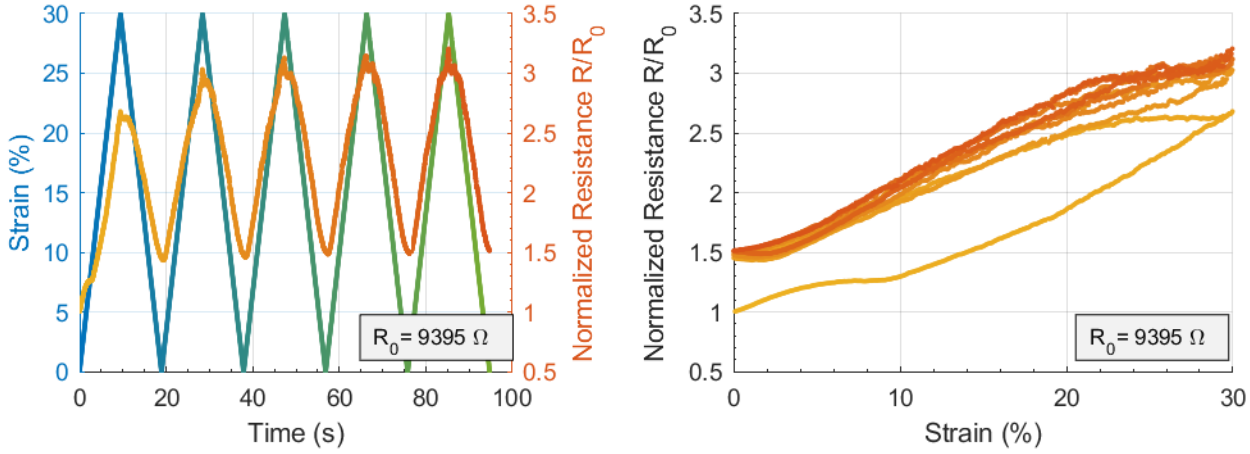

(a) (b)

Figure 4.20.: Exemplary strain cycle over time and relative resistance change ($\frac{R}{R_0}$) over time and strain of one LICC (LIC-Fiber)

The picture for the not stretched in figure 4.21a shows that the transferred fibers are arranged in lines and that in the stretched state (figure 4.21b) the fibers get horizontally separated and vertically compressed.

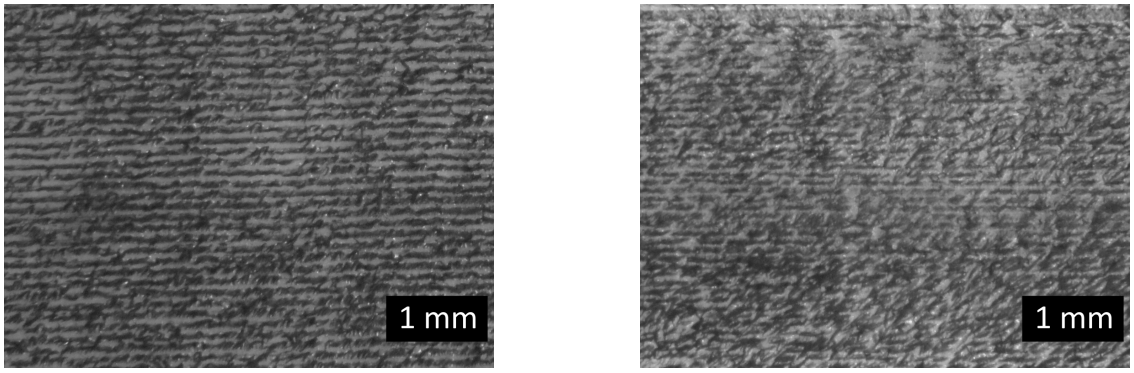

(a) not stretched (b) stretched

Figure 4.21.: Pictures of one LICC (LIC-Fiber) showing its not stretched and stretched state taken with a microscope

The statistics from all samples shown in table 4.9 show that the starting resistance is rather high with a value of $16 \pm 7\,\mathrm{k\Omega}$ but that this is a good stretchable conductor where the relative resistance change at 30 % strain is at $4.63 \pm 1.29\,\mathrm{R_0}$ and the resistance when relaxed again is at a stable value of $1.5\,\mathrm{R_0}$. Some samples broke at a strain of 45 % but recovered back to a resistance of $2.5\,\mathrm{R_0}$ after one stretching cycle to 100 % strain.

Table 4.9.: Statistical results of the LIC-Fiber conductor for different stretching cycles with R_0 the starting resistance and the relative resistance $\frac{R}{R_0}$ for the stretched and relaxed state

Strain (%)	R_0 (kΩ)	R/R_0 Stretched	R/R_0 Relaxed
5	15.7 ± 6.8	1.26 ± 0.07	1.16 ± 0.06
10	15.9 ± 6.9	1.52 ± 0.07	1.24 ± 0.04
30	16.7 ± 6.9	4.63 ± 1.29	1.53 ± 0.04
100	19.8 ± 7.7	broken at 45%	2.67 ± 0.29

4.4.4. Composite Conductor

After seeing the results for the LIC-Fiber conductor the idea for a combination of both types was born. The basic idea was to enhance the conductivity of the conductor while maintaining the behavior for the stretching. For this three layers of PEDOT:PSS (PJET700N) with a drop spacing of 35 µm were printed on top of the LIC-Fiber conductor and tested with the electromechanical stretching setup.

The results are shown in an exemplary plot in figure 4.22 where the starting resistance R_0 is around 1 kΩ. The stretching behavior in figure 4.22b seems to be a combination of the one from the LIC-Fiber and the PEDOT:PSS conductor as anticipated. After the first cycle a kind of steady state is reached which is superimposed with the increase of resistance seen from the PEDOT:PSS conductor. The resistance for the stretched state is around $3\,R_0$ and for the relaxed state around $2\,R_0$.

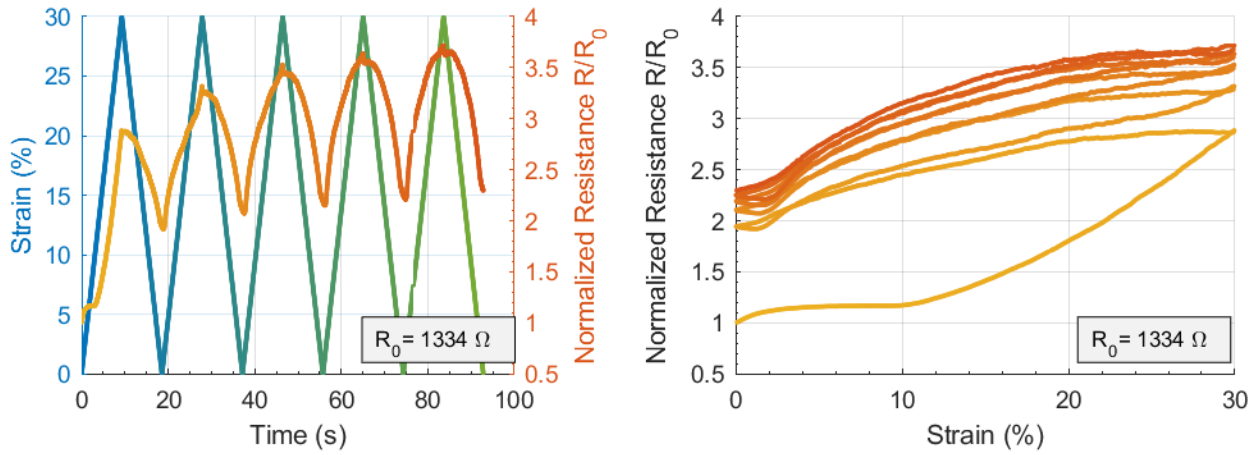

(a) (b)

Figure 4.22.: Exemplary strain cycle over time and relative resistance change ($\frac{R}{R_0}$) over time and strain of one composite conductor (LIC-Fiber + PEDOT:PSS)

The statistic shown in table 4.10 shows that the starting resistance with $1.4 \pm 0.4\,R_0$ is rather small. Although the stretched and relaxed resistance are not that far apart ($3\,R_0$ respectively $2.16\,R_0$) it seems to be a good trade-off between stretchability and conductivity. A notable fact is that the conductor could be stretched up to 100 % strain without being destroyed ($R \approx 20\,R_0$) and recovered to a value of around $3\,R_0$.

Table 4.10.: Statistical results of the composite conductor for different stretching cycles with R_0 the starting resistance and the relative resistance $\frac{R}{R_0}$ for the stretched and relaxed state

Strain (%)	R_0 (Ω)	R/R_0 Stretched	R/R_0 Relaxed
5	1.4 ± 0.4	1.11 ± 0.01	1.10 ± 0.01
10	1.5 ± 0.4	1.31 ± 0.07	1.27 ± 0.04
30	1.8 ± 0.4	2.99 ± 0.46	2.16 ± 0.20
100	3.3 ± 0.8	20.3 ± 4.6	3.26 ± 0.31

4.5. Electrocardiography Recording

For the recording of the ECG signal the Ag/AgCl and the MA electrode were placed on the positions shown in figure 3.22. In figure 4.23 the two electrodes are shown after they were placed on the right arm. The MA electrode is barely visible except for the red connector. In contrast to this the white Ag/AgCl electrode looks bulky and very prominent.
The only problem with the MA electrode is the connector and the cable. Because the electrode is so thin and soft the force from the weight of the cable causes distortion of the material. But this was a problem of this setup and will not be present in the final version.

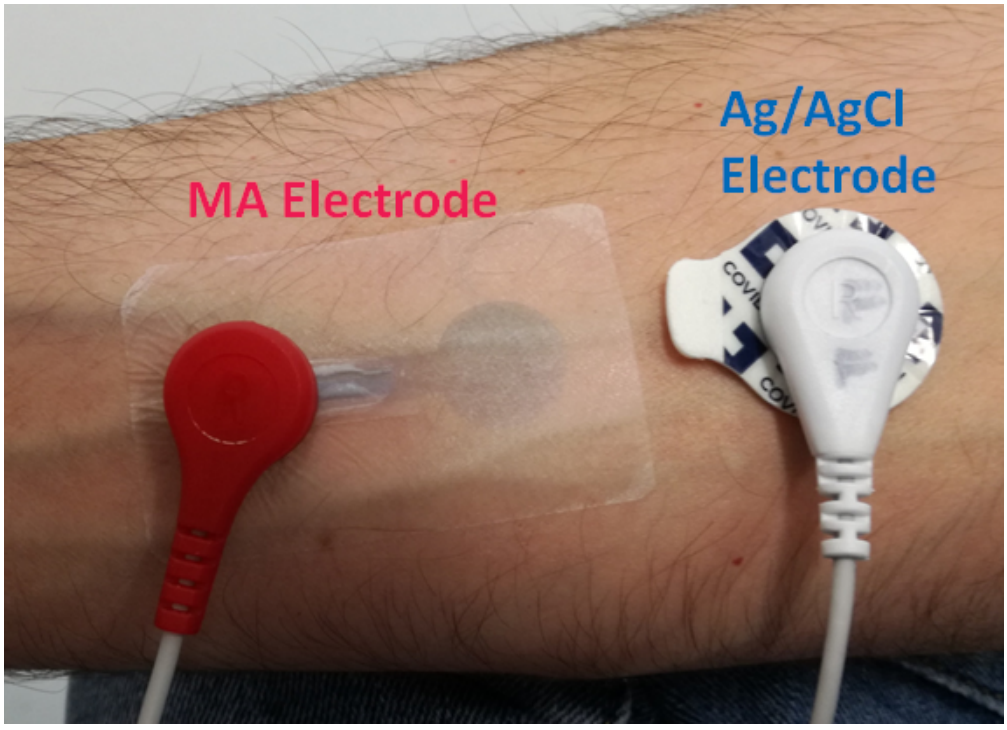

Figure 4.23.: Comparison between MA electrode prototype and a commercially available Ag/AgCl electrode

As explained before, two different measurements were done.
The first measurement shown in figure 4.24a was done asynchronous and this is why the beats are not aligned and the time is in arbitrary units because of some software issues. In this plot the ECG signal recorded with the MA electrode has very prominent peaks, but a bigger noise compared to the Ag/AgCl electrode. Nonetheless, all features shown in figure 2.1 can be observed in both recordings.

The latest measurement shown in figure 4.24b was done with a synchronous two channel setup and so both recordings of the two electrodes were measured at the same time and so all peaks are aligned. The noise in this measurement is much smaller as before in both recordings. However, the peak size of the MA electrode is smaller than the one from the Ag/AgCl electrode. Again, all features of the ECG recording can be clearly observed in both recordings.
Further it should be noted that the differences in amplitude and noise level can be from many influential factors. One big difference for these two plots was the test subject which were two different persons. During the experiments a big influence from the skin type could be observed.

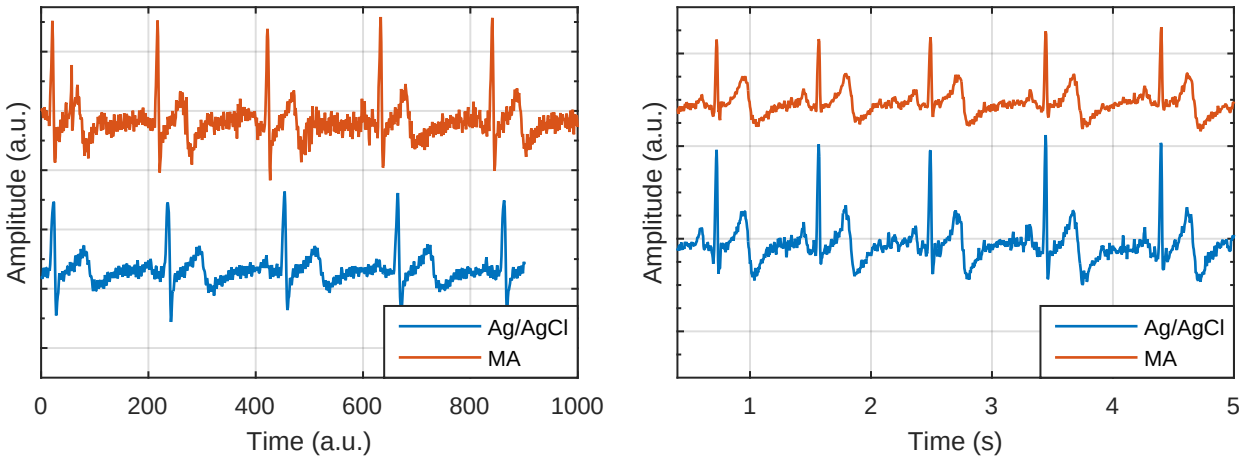

(a) Asynchronous ECG recording

(b) Synchronous ECG recording

Figure 4.24.: ECG recordings done with a commercially Ag/AgCl and a MA electrode

5. Miscellaneous

This section is about miscellaneous things that were done during this thesis but were not directly connected to the scope of this thesis.

5.1. Demonstrator for "Lange Nacht der Forschung"

For the "Lange Nacht der Forschung" a demonstrator for EMG detection was designed. The prototype electrodes were used to record muscle activation of the forearm while grasping and compressing a ball. This signal was recorded with the Arduino microcontroller and was used to control a small RC car. If a certain threshold of EMG signal (the grasping of the ball) was reached the car was accelerated and if the forearm was relaxed (threshold not reached) the car was stopped.

The purpose of this was to show children that this electrodes could be used to control devices, or in the case of disabled persons they could be used to control prosthetics replacing missing limbs.

5.2. Multi-layer Device through VIAS

During the experiments done with the laser cutter/engraver and the medical adhesive, especially the sample preparation, the idea for vertical interconnect accesses (VIAS) came up. The basic idea was to laser small holes into the medical adhesive and try to fill them with conductive ink. This would make it possible to produce multi-layer devices without the need of other production steps or machines. The laser settings used for the VIAS are the following: Power = 21 %, Speed = 2.5 %, PPI = 10.

The first trails showed that it was possible to produce VIAS and connect films of PEDOT:PSS from one layer to another one. The resistance of this VIAS was a few kΩ and looked promising.

In figure 5.1 pictures taken with the SEM show some VIAS with printed PEDOT:PSS. The first picture shows an overview with a measurement tip on the top left. It shows an array of five by five holes but it has to noted that the laser made two holes per point inserted into the program. This could unfortunately not be changed but it was still okay for the purpose. The second picture (figure 5.1b) shows one of these hole pairs with a higher magnification and a hole diameter of around 100 µm. The edges of the holes can already be seen in this picture which are magnified in figure 5.1c. In this picture it is possible to see the ink covering some of the hole walls which are responsible for the connection of the two layers.

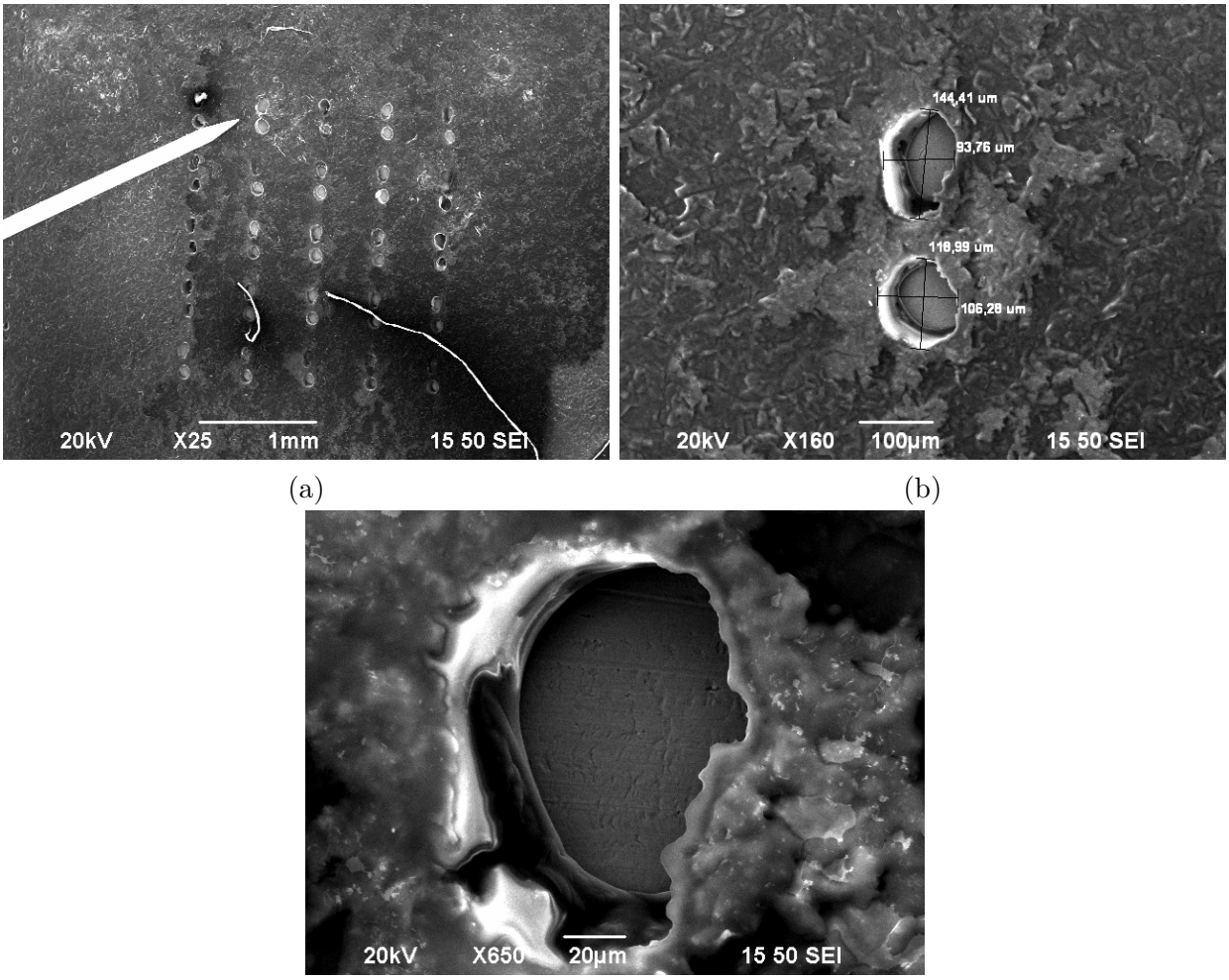

(a) (b)

(c)

Figure 5.1.: Pictures of the PEDOT:PSS VIAS taken with a SEM

For a demonstrator a simple multi-layer embedded LED was made. Figure 5.2a shows a simple sketch of the three layers of which the demonstrator was made. Layer 1 is a glass slide with two copper stripes for the connection to the power supply. Layer 2 is a layer of medical adhesive with the VIAS and both sides printed with PEDOT:PSS after making the holes. On layer 3 tracks were printed with PEDOT:PSS onto the medical adhesive and a LED was placed in between. All three layers were stacked on top of each other and connected to the power supply. In figure 5.2 the powered LED and therefore working VIAS are shown.

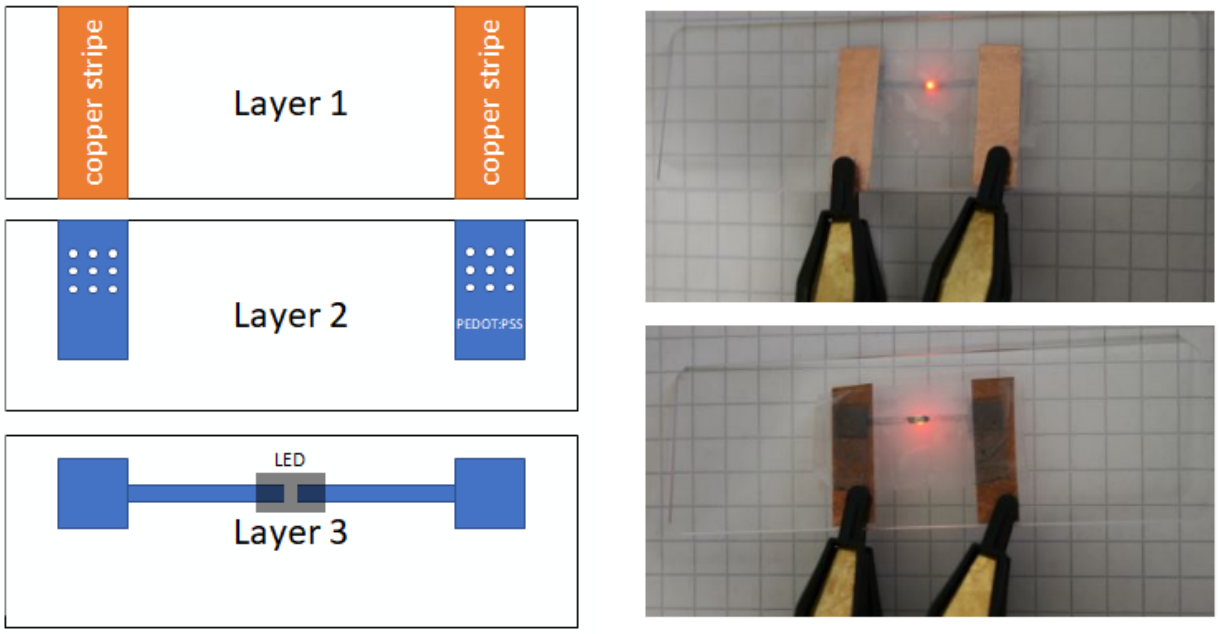

(a) Sketch of the demonstrator with embedded LED

(b) Powered embedded LED connected through VIAS

Figure 5.2.: PEDOT:PSS VIAS demonstrator with an LED embedded between two layers of medical adhesive

These VIAS could be used to make the next generation of MA-electrodes. Such a electrode is shown in figure 5.3. The VIAS are used to connect the printed ECG-electrode to a wireless communication chip which sends the recorded signals to a personal health monitor. With this it is possible to supersede the cables for data transfer and enables embedded electrodes with integrated electronics.

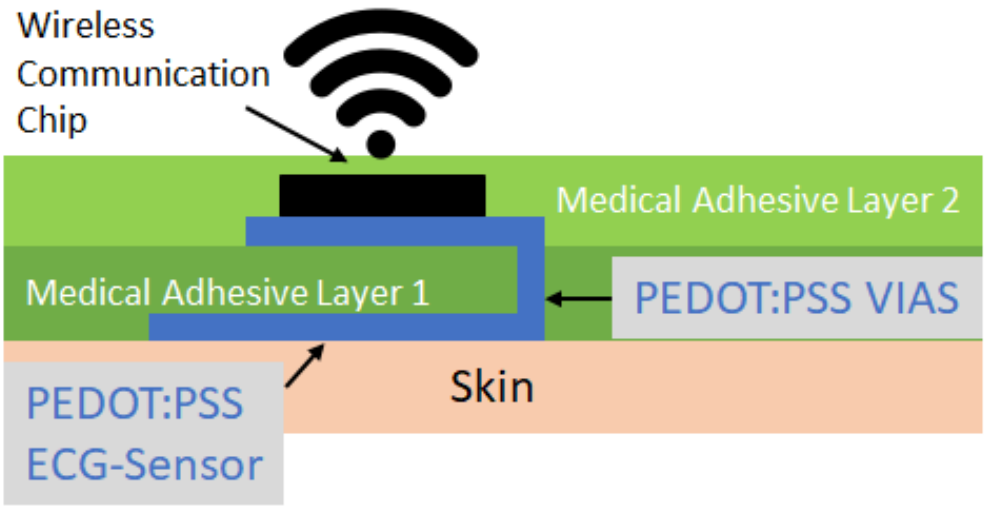

Figure 5.3.: Sketch of an embedded ECG electrode realized with PEDOT:PSS VIAS for connecting the different layers

5.3. Response to Humidity

During the measurements with the LICC and the electromechanical stretching setup a change in resistance was noticed while working close to the samples. After some investigation it turned out the humid air of the breath was the cause of the resistance change. This called for further investigation and an array of LICC was made on top of a glass slide as shown in figure 5.4. For this the LIC-Flat was transferred onto the medical adhesive and was placed onto the glass slide with the contacts. This electrode array was put into a custom humidity chamber and some measurements were done. One of these measurements is shown in figure 5.5 and shows that the resistance follows the change of humidity. Whilst the change for increasing humidity is rather slow, the change for decreasing humidity is very rapid. It seems that the LICC on the medical adhesive could be used as a very cheap humidity sensor and should be investigated in more detail.

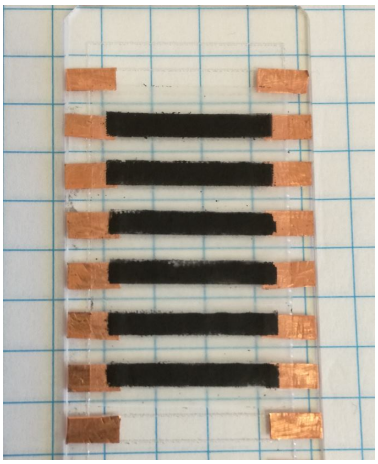

Figure 5.4.: Array of LIC stripes on medical adhesive pasted onto a glass slide with copper contacts

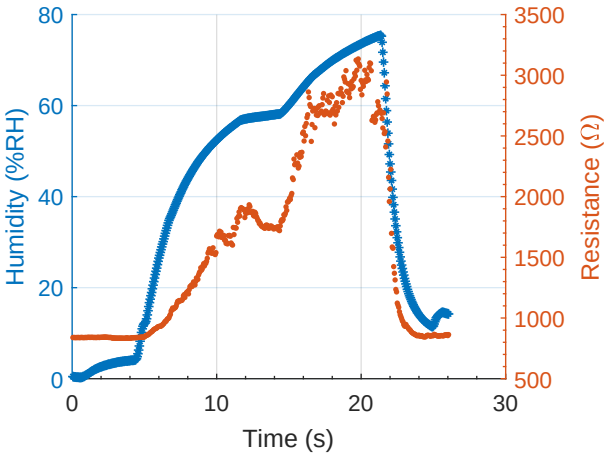

Figure 5.5.: Humidity response curve of the LICC

6. Discussion and Conclusion

Looking at the results of *Section 4.1 Characterization of Conductive Inks* it showed that all inks have the predicted dependence on drop spacing and number of printed layers. With an increasing drop spacing the thickness and therefore the conductivity decreased. If the number of printed layers was increased the thickness and the conductivity were increased. Also, the conductivity of the films printed onto glass had a higher conductivity than the ones on the medical adhesive. This is probably because of the surface roughness of the medical adhesive which is preventing a flat film. The measurements also showed that with three or five layers the conductivity reached a saturation value which is in agreement with the specified conductivity of around 500 to 650 S/cm from the manufacturer.

Regarding the laser induced carbon, it was shown that it was possible to scribe conductive tracks into the polyimide and transferred them onto the medical adhesive and kept a part of the conductivity. Although the conductivity ($\sigma = 18 \pm 4$ S/cm) for LIC-Flat was reduced to around 10 % after transfer which was because of the compression and destruction of the 3D porous structure. The LIC-Fiber could not be characterized because of its structure which is discussed in the next paragraph.

The pictures taken with the SEM showed that the 2 power settings (P=10, 20 % of the 30 W laser) have a very different morphology. The LIC-Flat (P=10 %) showed a surface which seems flat with trenches caused by the laser irradiation. At the edges of this trenches very small fibers were found.
In comparison the LIC-Fiber showed a surface with macroscopic fiber cones consisting of fibers with a length of a few hundred µm and a diameter of a few hundred nm which are aligned in a direction.
After taking a look at the LIC bulk, which was transferred onto the medical adhesive (to get a look at the bottom surface, see figure 3.8) the porous nanostructure mentioned by [10] could be confirmed.
The LIC-Fiber transferred onto the medical adhesive showed that the orientation of the fibers was lost and the fibers were partly destroyed by the transfer process. Also the coverage of the fibers was not 100 % and could be improved.

The calibration of the mechanical stretching setup and the verification with a silicon rubber (Elastosil®) done by Michael Gobald ([15]) showed that the setup was working as intended. The components and software used for the design and implementation are stated in section 3.3.

This setup was used to characterize the mechanical properties of the medical adhesive and the electromechanical properties of the stretchable conductors consisting of conductive films deposited onto the medical adhesive.
The medical adhesive which is polyurethane plus an adhesive layer showed typical behavior for thermoplastic polyurethane as stated in [17]. Cyclic softening and a plastic deformation (rule of thumb: 10 % of the strain value) were observed. Although the interesting region for epidermal electronics (strain of around 10 %) showed a rather elastic behavior with very small plastic deformations.

The two stretchable conductors, ink-jet printed conductors (IPC) and laser induced carbon conductors (LICC) were tested with the stretching setup.
The ink-jet printed conductors showed a very unreliable stretching behavior, with some samples breaking at 2 % strain and others at values above 10 %. The measurements showed the PJET700 was more stretchable and more reliable than PJET700N. Although the starting resistance of around 1 kΩ was a good value the stretchability was not good at all.
Compared to this the LICC showed a pretty good stretchability but either needed to be very thick to reach the conductivity (in the case of LIC-Flat) of the IPC or had a very high starting resistance of 10 kΩ in the case of LIC-Fiber.

After inspection with the microscope the behavior of the IPC could be explained by cracks forming while stretching (see figure 4.14). This cracks can come from the treatment of the medical adhesive with plasma and resulting in a brittle surface which enhances the formation of cracks (see [9]) or the formulation of these PEDOT:PSS inks are not good for stretchability. So the idea of combining the LIC-Fiber and PEDOT:PSS was born. The basic idea was to bridge the cracks formed by PEDOT:PSS with the fibers. For these three layers of PJET700N were deposited onto a LIC-Fiber sample and the measurements were performed again. And the result showed that the conductivity of the film and the stretchability of the fibers were present. This showed that the properties of the two conductors could be superimposed and a good stretchable conductor (stretchable over 100 % strain) could be made. This could solve problems which were encountered with the ECG electrode prototype discussed in the next paragraph.

Another part of this thesis was to design and test an electrode prototype based on the medical adhesive and a PEDOT:PSS film. The recording plotted in figure 4.24 shows that it was possible to record good ECG signals with the electrode prototype and that the signal quality was comparable to the one of the standard Ag/AgCl electrodes.

Quickly summing up the chapter with the miscellaneous experiments it was shown that simple vertical interconnect accesses (short VIAS) could be produced with the laser engraver and printing PEDOT:PSS on it. For a demonstration a LED embedded in medical adhesive was powered through this PEDOT:PSS VIAS.
Another phenomenon observed during the handling with the LICC samples was that the resistance changed significantly when breathing onto the sample. This was the reason why a quick test with the LIC was made and it showed that the resistance was indeed humidity dependent. This needs of course more sophisticated experiments and investigation.

Concluding all measurements it can be stated that modern skin contact electrodes can be manufactured out of commercially available medical materials which are retrofitted with a conductive film (be it PEDOT:PSS or some other biocompatible conductor). Although some problems like the stretchability of PEDOT:PSS or the connectivity to external devices still need some improvement. One improvement for stretchability could be the use of composite conductors such as the combination of PEDOT:PSS and LIC-Fibers. Regarding the connectivity problem the VIAS briefly investigated in *Section 5.2 Multi-layer Device through VIAS* could be used to make fully integrated electrodes with wireless communication as shown in figure 5.3.

Bibliography

1. Ferrari, L. M. *et al.* Ultraconformable Temporary Tattoo Electrodes for Electrophysiology. *Advanced Science* **5** (2018).
2. Liu, Y., Pharr, M. & Salvatore, G. A. Lab-on-Skin: A Review of Flexible and Stretchable Electronics for Wearable Health Monitoring. *ACS Nano* **11,** 9614–9635. ISSN: 1936-0851, 1936-086X (Oct. 24, 2017).
3. Kim, D.-H. *et al.* Epidermal electronics. *science* **333,** 838–843 (2011).
4. Hall, J. E. *Textbook of Medical Physiology* 1113 pp. ISBN: 978-1-4377-2674-9 (Elsevier Health Sciences, July 19, 2010).
5. Meyers, M. A. & Chen, P.-Y. *Biological Materials Science: Biological Materials, Bioinspired Materials, and Biomaterials* 647 pp. ISBN: 978-1-139-95220-0 (Cambridge University Press, July 31, 2014).
6. Greco, F. *et al.* Ultra-thin conductive free-standing PEDOT/PSS nanofilms. *Soft Matter* **7,** 10642–10650 (2011).
7. Balint, R., Cassidy, N. J. & Cartmell, S. H. Conductive polymers: towards a smart biomaterial for tissue engineering. *Acta biomaterialia* **10,** 2341–2353 (2014).
8. Lipomi, D. J. *et al.* Electronic Properties of Transparent Conductive Films of PEDOT:PSS on Stretchable Substrates. *Chemistry of Materials* **24,** 373–382. ISSN: 0897-4756, 1520-5002 (Jan. 24, 2012).
9. Vosgueritchian, M., Lipomi, D. J. & Bao, Z. Highly Conductive and Transparent PEDOT:PSS Films with a Fluorosurfactant for Stretchable and Flexible Transparent Electrodes. *Advanced Functional Materials* **22,** 421–428. ISSN: 1616-3028 (Jan. 25, 2012).
10. Lin, J. *et al.* Laser-induced porous graphene films from commercial polymers. *Nature communications* **5,** 5714 (2014).
11. Topsoe, H. Geometric factors in four point resistivity measurement. *Bulletin* **472,** 63 (1968).
12. *Heraeus Group* `www.heraeus.com` (2019).
13. Mitterling, J. *A Map to LIC* Bachelor Thesis (TU Graz, 2018).
14. Ye, R., James, D. K. & Tour, J. M. Laser-Induced Graphene. *Accounts of Chemical Research* (2018).
15. Gobald, M. *Testing of a materials tensile testing device for the investigation of the mechanical and conductive properties of stretchable conductors* Bachelor Thesis (TU Graz, 2018).
16. Wacker Chemie AG. *Ultrathin silicone film for high-precision solutions* `https://www.wacker.com/cms/media/publications/downloads/7091_EN.pdf` (2018).
17. Qi, H. J. & Boyce, M. C. Stress–strain behavior of thermoplastic polyurethanes. *Mechanics of Materials* **37,** 817–839 (2005).

A. Room for Improvements

During the experiments some problems were encountered, but there was not enough time to solve them. This section is to list all the problems and their possible solution for future use.

The electromechanical stretching setup can be improved in a few ways. Starting with the measurement speed of the Keithley which is used to measure the resistance during the measurement. The problem is that one measurement with this devices takes around 30 ms and this is very slow. This is limiting the maximum speed for the measurement to around $0.5\,\frac{\mathrm{mm}}{\mathrm{s}}$ because of the data points per second recorded. With faster measurements the data point density is very small and a lot of information is lost. In figure 4.12a the limit can already be seen. This was a very short measurement (about 15 s with a speed of $0.5\,\frac{\mathrm{mm}}{\mathrm{s}}$) and the single data points can be spotted.
A possible solution could be the use of a different source meter (a simple Keithley2400) or maybe there is the possibility to set the measurement time or internal averaging. This is something with a high priority to fix because it is trimming the capabilities of the setup a lot.

One thing that can be improved is the measurement of the sample length. Maybe some sensor (strain gauge, ultrasonic or laser) can be used to determine the position of the carriage and therefore the length of the sample. This would eliminate the step of measuring the distance with a slide gauge and minimize the errors made by the operator.

Regarding the operation also an algorithm that can be used to detect the zero force point (no stretching of the sample) could improve the usability of the setup a lot. At the moment one has to connect a handheld voltmeter to measure the voltage of the load cell. The screw which moves the carriage is moved by hand until the voltmeter shows a voltage of 0 V.

B. Appendix

B.1. Drop Spacing Conversion

Table B.1.: Conversion from drop spacing (DSP in µm) in DPI

DSP (µm)	DPI
5	5080
10	2540
15	1693.33
20	1270
25	1016
30	846.67
35	725.71
40	635
45	564.44
50	508

B.2. Thickness Measurement of PEDOT:PSS Ink

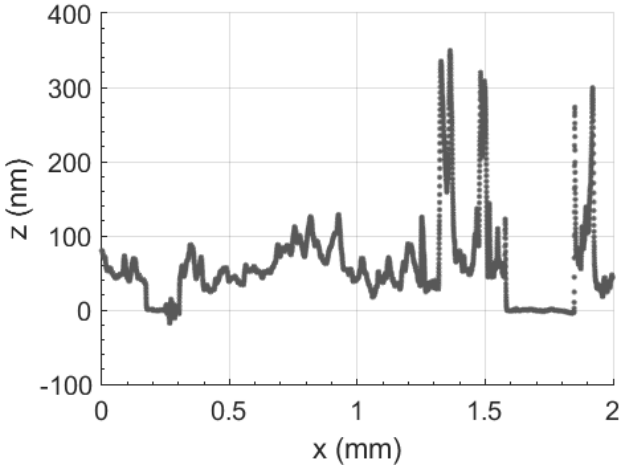

Figure B.1.: A measurement of thickness to show that the film surfaces of PJET700 and PJET700N are very rough and result in big uncertainties for the thickness

B.3. How to Operate the Stretcher

A small guide on how to use the Stretcher:

1. Plug in the power supply
2. Turn on the Keithley 2601B
3. Make sure that the Arduino is running on „StepperController V5“ software
4. Start the Stretcher V2 software
5. Press the Connect button
6. LOAD or CREATE a stretch-file (elongation in %, speed, delay)
7. Typ. settings. $\epsilon = 5, 10, 30, 100$ %
8. Speed = 500, 1000, 2000, 5000, 10000
9. Equation for speed in $\frac{\text{mm}}{\text{s}}$: $(5.32 * 10^{-4}) * X)$
10. Delay for investigation of long time behavior
11. Sample preparation
12. Mount the sample onto the paper frame
13. Carefully remove holding brackets
14. Mount the frame onto the carriage
15. In case of Fixomull remove the plastic liner
16. Fasten the brackets again
17. Cut the paper frame
18. Find the 0 Force point with the help of the multimeter (find 0V)
19. Measure the length of the sample between the brackets
20. Press the Start button and fill out the sample geometry form
21. After the measurement a save prompt will be opened

B.4. ECG Recording Program

```
#include <FlexiTimer2.h>

#define SAMPFREQ 250  // ADC sampling rate 250
#define TIMER2VAL (1000/(SAMPFREQ))  // Set 250Hz sampling frequency
   -> timerval in ms

volatile unsigned char Channel_0 = 0;
volatile unsigned char Channel_1 = 1;
volatile unsigned int ADC_Value_0 = 0;
volatile unsigned int ADC_Value_1 = 0;

void setup() {
        noInterrupts(); // Disable all interrupts before initialization
        FlexiTimer2::set(TIMER2VAL, Timer2_Overflow); // Initialize and
            start the timer
        FlexiTimer2::start();
        Serial.begin(115200); // Start serial communication
        interrupts(); // Enable all interrupts after initialization has
            been completed
}

void Timer2_Overflow()
{
        // read out ADC Values
        ADC_Value_0 = analogRead(Channel_0);
        ADC_Value_1 = analogRead(Channel_1);

        // send ADC_Value over serial
        Serial.print(ADC_Value_0);
        Serial.print(",");
        Serial.println(ADC_Value_1);
}

void loop() {
        __asm__ __volatile__ ("sleep");
}
```

Listing B.1: Arduino code for the recording of the ECG signals with the Olimex-ECG-Shield